Icarus **140**, 243–264 (1999)
Article ID icar.1999.6129, available online at http://www.idealibrary.com on IDEAL®

Active Volcanism on Io: Global Distribution and Variations in Activity

Rosaly Lopes-Gautier

Jet Propulsion Laboratory, California Institute of Technology, Pasadena, California 91109
E-mail: rlopes@issac.jpl.nasa.gov

Alfred S. McEwen

Department of Planetary Sciences, Lunar and Planetary Laboratory, University of Arizona, P. O. Box 210092, Tucson, Arizona 85721-0092

William B. Smythe

Jet Propulsion Laboratory, California Institute of Technology, Pasadena, California 91109

P. E. Geissler

Department of Planetary Sciences, Lunar and Planetary Laboratory, University of Arizona, P. O. Box 210092, Tucson, Arizona 85721-0092

L. Kamp and A. G. Davies

Jet Propulsion Laboratory, California Institute of Technology, Pasadena, California 91109

J. R. Spencer

Lowell Observatory, Flagstaff, Arizona 86001

L. Keszthelyi

Department of Planetary Sciences, Lunar and Planetary Laboratory, University of Arizona, P. O. Box 210092, Tucson, Arizona 85721-0092

R. Carlson

Jet Propulsion Laboratory, California Institute of Technology, Pasadena, California 91109

F. E. Leader and R. Mehlman

Institute of Geophysics and Planetary Physics, University of California—Los Angeles, Los Angeles, California 90095

L. Soderblom

Branch of Astrogeologic Studies, U.S. Geological Survey, Flagstaff, Arizona 86001

and

The Galileo NIMS and SSI Teams

Received June 23, 1998; revised February 10, 1999

Io's volcanic activity has been monitored by instruments aboard the Galileo spacecraft since June 28, 1996. We present results from observations by the near-infrared mapping spectrometer (NIMS) for the first 10 orbits of Galileo, correlate them with results from the Solid State Imaging System (SSI) and from groundbased observations, and compare them to what was known about Io's volcanic activity from observations made during the two Voyager flybys in 1979. A total of 61 active volcanic centers have been identified from Voyager, groundbased, and Galileo observations. Of these, 41 are hot spots detected by NIMS and/or SSI. Another 25 locations were identified as possible active volcanic centers, mostly on the basis of observed surface changes. Hot spots are correlated with surface colors, particularly dark and red deposits, and generally anti-correlated with white, SO_2-rich areas. Surface features corresponding to the hot spots, mostly calderas or flows, were identified

0019-1035/99 $30.00

from Galileo and Voyager images. Hot spot temperatures obtained from both NIMS and SSI are consistent with silicate volcanism, which appears to be widespread on Io. Two types of hot spot activity are present: persistent-type activity, lasting from months to years, and sporadic events, which may represent either short-lived activity or low-level activity that occasionally flares up. Sporadic events are not often detected, but may make an important contribution to Io's heat flow and resurfacing. The distribution of active volcanic centers on the surface does not show any clear correlation with latitude, longitude, Voyager-derived global topography, or heat flow patterns predicted by the asthenosphere and deep mantle tidal dissipation models. However, persistent hot spots and active plumes are concentrated toward lower latitudes, and this distribution favors the asthenosphere rather than the deep mantle tidal dissipation model.

Key Words: **Io; volcanism; infrared observations.**

1. INTRODUCTION

One of the major objectives of the Galileo mission is to study Io's volcanic activity and how it varies with time. Active volcanism on Io was discovered from images and infrared measurements taken by the Voyager 1 spacecraft during its flyby of the Jupiter system in 1979 (e.g., Smith *et al.* 1979). Four months later, the Voyager 2 flyby revealed that some major changes had taken place on Io, including the apparent shutoff of the Pele plume and the filling of the fallout ring around Pele. Analysis of Voyager 1 IRIS data (Pearl and Sinton 1982, McEwen *et al.* 1992a,b) showed at least 22 hot spots over about a third of the surface. The cameras (ISS) aboard the two Voyager spacecraft detected a total of nine active plumes (Strom *et al.* 1981, McEwen *et al.* 1989). All of the plume sites that were also observed by IRIS showed the presence of hot spots.

Since Voyager, Io's activity has been monitored by observations from groundbased telescopes (e.g., Veeder *et al.* 1994, Goguen *et al.* 1988, Spencer *et al.* 1997a). Hot spot detections from groundbased observations were summarized by Spencer and Schneider (1996) and Spencer *et al.* (1997a).

The Galileo mission has provided the unprecedented opportunity to monitor the activity of Io's volcanoes from Jupiter orbit. During its two-year primary mission, from December 1995 to December 1997, Galileo has encountered Ganymede, Callisto, and Europa. The spacecraft has come no closer to Io than 240,000 km during each orbit, except at Jupiter Orbit Insertion (JOI) when no remote sensing observations were taken. Closer ranges are planned during the Galileo Europa Mission (GEM), including two close flybys of Io at the end of the mission in 1999. The near-infrared mapping spectrometer (NIMS) has observed Io at least twice during each of Galileo's orbits, starting on June 28, 1996. The main objectives of the NIMS observations of Io are (i) to investigate the distribution and temporal variability of hot spots on Io's surface (Lopes-Gautier *et al.* 1997a) and (ii) to determine Io's surface composition and the distribution of SO_2 on the surface (Carlson *et al.* 1997).

The Solid State Imaging System (SSI) aboard Galileo is investigating Io's geologic features, plume activity, surface colors, and high-temperature hot spot activity (McEwen *et al.* 1997, 1998a,b; Carr *et al.* 1998; Simonelli *et al.* 1997; Geissler *et al.* 1999). SSI's spatial resolution is 50 times that of NIMS, enabling it to detect smaller hot spots than NIMS can, as long as the temperatures of these hot spots are sufficiently high to be detectable using the camera. SSI can detect hot spots having a minimum temperature of 700 K if the pixel is filled (McEwen *et al.* 1997). The NIMS wavelength range, from 0.7 to 5.2 μm, enables it to detect cooler hot spots than SSI, down to 180 K if the hot spot fills a NIMS pixel (Smythe *et al.* 1995). All of the NIMS pixels in the observations obtained so far are greater than 14,884 km^2, significantly larger than hot spot areas, which are typically only a few square kilometers (Lopes-Gautier *et al.* 1997). The coolest temperatures obtained from a single blackbody fit to NIMS data have been about 300 K.

The combination of NIMS and SSI observations is of great value for the study of Io's volcanic activity. The two instruments provide complementary data for investigating the relationship between hot spot activity, plume activity, and surface geology. We present here the results of the NIMS search for new and recurrent hot spots on Io from observations taken during Galileo's first 10 orbits. We combine the NIMS results with those from the SSI observations (McEwen *et al.* 1997, 1998a), those from groundbased observations obtained during and prior to the Galileo mission (summarized in Spencer *et al.* 1997a), and those obtained from Voyager data (Pearl and Sinton 1982, McEwen *et al.* 1992a,b). The combination of these data sets provides our most complete view to date of the global distribution and temporal variability of Io's hot spot activity.

2. IO OBSERVATIONS BY GALILEO NIMS AND SSI

The NIMS instrument has been described previously by Carlson *et al.* (1992) and Smythe *et al.* (1995). NIMS includes a spectrometer with a scanning grating and spans the wavelength range 0.7 to 5.2 μm, therefore measuring both reflected sunlight and thermal emission. NIMS forms spectra with 17 detectors in combination with a moving grating. The 17 wavelengths obtained for each grating position are acquired simultaneously, thus providing a "snapshot" spectrum of the target. Spectra obtained for different grating positions are not located precisely on the same spot on the planet, because of motion of the field of view relative to the surface during the time between grating steps (0.33 s). This motion has implications for the analysis of NIMS data, such as the variance of hot spot temperatures measured (Lopes-Gautier *et al.* 1997).

NIMS has observed Io at least twice per orbit during Galileo's orbits G1 through C10, corresponding to the period from June 28, 1996 to September 20, 1997. Most observations were taken within one to three days of closest approach in each orbit, covering all latitudes and either the whole disk or part of the disk. The NIMS global coverage of Io in these orbits had spatial

resolutions typically in the range 200–500 km/pixel. The highest spatial resolution was obtained on the anti-jovian hemisphere (122 km/pixel), while the poorest spatial resolution was on the Jupiter–facing hemisphere (for the swath 350W-0-40W the resolution was, at best, 516 km/pixel). Often, NIMS has taken pairs of observations close together in time, one covering Io's dayside and the other Io's nightside, to permit use of a more sensitive gain state for the nightside. Most observation modes return between 102 and 408 wavelengths. A small number of NIMS Io observations taken during the first few orbits returned fewer than 102 wavelengths, and are harder to interpret. The high radiation environment near Jupiter causes noise spikes to be introduced in the data, which must be removed before data analysis. The higher the number of wavelengths returned, the easier it is to identify and remove the radiation-induced noise.

The Galileo SSI instrument has been described by Belton *et al.* (1992) and by Klaasen *et al.* (1997). McEwen *et al.* (1998a) summarized observations taken during the first 10 orbits of Galileo and the major results from the observing campaign. Of particular interest to this paper are SSI's eclipse observations, taken when Io is in Jupiter's shadow. Long-exposure images are taken to search for high-temperature hot spots and diffuse atmospheric/plume glows. Use of SSI's clear (CLR) and 1-μm (1MC) filters on the same observation allows hot spot temperatures to be estimated (McEwen *et al.* 1998b). Eclipse observations were obtained by SSI in orbits G1, E4, E6, G7, G8, C9, C10, and E11.

3. DETECTION OF HOT SPOTS

The detection of hot spots by NIMS during the first four Galileo orbits (G1, G2, C3, and E4) was discussed by Lopes-Gautier *et al.* (1997a). Here we update the previous study to include NIMS results from the Galileo orbits E6, G7, G8, C9, and C10.

The NIMS search for hot spots consists of a pixel-by-pixel analysis of each observation. A pixel is considered to contain a hot spot when the positive slope of the spectrum between 3.5 and 5 μm is greater than that of all surrounding pixels. However, the pixels identified as hot spots in this search do not account for all of the thermal emission that NIMS detects from Io, as discussed by Lopes-Gautier *et al.* (1997a). A pixel-by-pixel thermal map of a NIMS observation of Io's nightside during the first orbit (Smythe *et al.* 1997) shows other NIMS pixels that have significant thermal output based on their increasing radiance from 3 to 5 μm. These pixels are not listed as pixels containing hot spots in our search because they fall in one of two categories. The first is when the thermal signal is relatively weak; that is, the local maximum is less than 5% greater than that of the surrounding pixels. This probably represents hot spots that are relatively small or cool, and further analysis and/or independent measurements are needed before they can be identified as hot spots. In the second category are the cases where a pixel has a significant thermal signal between 3 and 5 μm, but the output is less than that from neighboring pixels which were identified as hot spots. This may represent adjacent hot spots that cannot be fully resolved at the available spatial resolution, or energy that is distributed between pixels because of the instrument's point-spread function (Carlson *et al.* 1992). Because major hot spots are typically separated by less than 500 km, the hot spot detection methods used here are much less effective at 500 km/pixel than at 250 km/pixel.

All temperature–area calculations done so far show that Io's hot spots are subpixel at NIMS spatial resolutions. Pixel-by-pixel thermal maps using the method explained by Smythe *et al.* (1997, 1999) will clarify the existence of hot spots in the two categories above. The hot spot detections given in this paper should, therefore, be considered as the minimum number of hot spots detectable from NIMS data. In terms of power output measured from NIMS nightside data (Lopes-Gautier *et al.* 1999), the majority of hot spots detected fall in the range 10^{10} to 10^{11} W.

The positions of hot spots observed by NIMS in orbits G1 through C10 are listed in Table I. Also listed in Table I are: (i) positions of hot spots and plume sites detected from SSI eclipse data; (ii) positions of hot spots detected by Voyager IRIS and from groundbased observations and their possible correlation with NIMS and SSI hot spots; and (iii) positions and types of features on the surface that we infer to be the sources of the thermal emission detected by NIMS, SSI, IRIS, and groundbased observations. The hot spot latitudes and longitudes obtained from NIMS data were determined from the highest spatial resolution observations available for each region. The coordinates are the central coordinates of the NIMS pixels containing each hot spot. Errors listed correspond to half a NIMS field of view (i.e., half the pixel size). The corresponding positions derived from SSI hot spot detections (McEwen *et al.* 1997, 1998a), when available, are more precise because of the higher spatial resolution of the camera. Errors in latitude and longitude for SSI hot spot positions are usually less than 1° (McEwen *et al.* 1997). The positions of volcanic centers identified as the source areas for individual hot spots were taken from SSI images that show these surface features in detail. In all cases, these features are located within the error limits of the positions derived from NIMS data. The volcanic centers consist of calderas, flows, and/or plume deposits, and in every case show the presence of low-albedo material.

A total of 37 hot spots have been detected by NIMS, including 22 that were not known from Voyager or groundbased measurements. Most of these hot spots were detected by NIMS in the anti-jovian hemisphere, which was observed by Voyager at low spatial resolution. The anti-jovian hemisphere is also poorly observed from the ground, but it is where the NIMS spatial resolution is highest, due to the configuration of Galileo's orbits. SSI detected hot spots at 18 locations during orbits G1 through C10. This number is a minimum because (i) some bright pixels seen in SSI eclipse images have not yet been confirmed to be hot spots (Table II) and (ii) the hot spots at three of these locations span multiple hot spots. For the purpose of this analysis, we

TABLE I

Active Volcanic Centers on Io: Detections of Plumes and Hot Spots by Galileo, Voyager, and Groundbased Observations

Volcanic center	Location of candidate surface feature	SSI hotspot	Location Galileo NIMS	Voyager IRIS hot spot?	Ground-observed hot spot?	Plume? (V,G)	Surface Change?	Notes
Nusku Patera	63 S, 7 W			yes?		no	no	
Mbali Patera	32 S, 8 W			yes		no	no	Red deposits
Karei Patera?	2 N, 16 W	yes?			9608A ?	no	no	
Ukko Patera	32 N, 20 W				9508A ?	no	yes	
Uta Patera	35 S, 25 W			yes?	9606C ?	no	no	Very low albedo
Kanehekili-N&S	18 S, 37 W	14.5 S, 33.4 W 17.2 S, 35.5 W	12±10 S, 34±4 W		yes	G	yes	
Unnamed (N. Polar)	70±15 N, 35±15 W				9610A	no	yes	N. Polar changes seen by SSI, unclear if location consistent with hot spot detected from the ground
Janus Patera	3 S, 40 W	4 S, 39 W	4±5 S, 42±5 W		9606A ?	no	no	
Masubi	44 S, 55 W					V	yes	
Shamshu	10 S, 63 W		10±4 S, 67±4 W			no	no	
Zal Patera	41 N, 76 W	36.3 N, 76.1 W	43±7 N, 78±10 W			no	yes	Bright red deposits
Hi'iaka Patera	2 S, 79 W		1±4 S, 76±4 W		yes	no	yes	
Gish Bar Patera	17 N, 90 W	16.3 N, 91 W	16±4 N, 89±5 W			no	no	
Sigurd Patera	5 S, 97 W		5±4 S, 100±4 W			no	no	
Unnamed (S. Sigurd)	16 S, 98 W		15±3 S, 97±3 W			no	no	
Monan Patera	19 N, 106 W		19±3 N, 106±4 W			no	no	
Altjirra Patera	35 S, 109 W		33±4 S, 108±4 W	yes-same as Malik?		no	yes	Bright red deposits
Amirani	25 N, 116 W	23.2 N, 116.3 W	27±4 N, 112±4 W	yes		V,G	yes	Bright red deposits
Maui	20 N, 122 W		19±3 N, 122±3 W	yes-same as Amirani?		V	yes?	Voyager plume obscures surface
Malik Patera	35 S, 128 W		35±3 S, 127±3 W	yes		no	no	Bright red deposits
Unnamed (N. Polar)	65 N, 141 W	65.2 N, 132 W				no	no	
Tupan Patera	18 S, 141 W		17±3 S, 141±3 W			no	no	Bright red deposits
Unnamed (9606W)	32 N, 147 W		36±6 N, 147±6 W			no	yes	Bright red deposits
Shamash Patera	34 S, 153 W		33±6 S, 157±6 W	yes-same as Malik?		no	no	
Prometheus	2 S, 154 W		1±3 S, 155±3 W			V,G	yes	Bright red deposits
Culann Patera	19 S, 160 W		18±3 S, 163±3 W			G?	yes	Bright red deposits
Zamama	18 N, 173 W	18.9 N, 172 W	21±3 N, 173±3 W			G	yes	Bright red deposits
Volund	23 N, 176 W		25±3 N, 174±3 W	yes		V	yes	
Aidne Patera	1 S, 177 W		2±3 S, 178±3 W			no	yes	
Fo Patera	40 N, 192 W	40.1 N, 200.8 W	39±3 N, 191±3 W			no	yes	
Sethlaus Patera	52 S, 194 W		50±3 S, 195±3 W			no	no	Red deposits
Rata Patera	35 S, 199 W		35±3 S, 199±3 W			no	no	Red deposits
Lei-Kung Fluctus	36 N, 203 W		37±3 N, 206±3 W			no	no	Bright red deposits
Isum Patera-N&S	29 N, 209 W 30.3 N, 206.8 W	32.9 N, 204.7 W	31±3 N, 207±3 W	yes	9510A ?	no	no	Bright red deposits
Marduk	27 S, 209 W	27.1 S, 209.1 W	26±3 S, 212±3 W	yes		V,G	yes	Bright red deposits
Kurdalagon Patera	50 S, 218 W		47±3 S, 219±3 W			no	no	Red deposits
Unnamed (9611A)	2 S, 218 W		2±3 S, 218±3 W			no	no	
Mulungu Patera	17 N, 218 W	17.6 N, 216.8 W	17±3 N, 219±3 W		9510A ?	no	no	
Reiden Patera	13 S, 236 W	12.5 S, 234.9 W				no	no	
Pillan Patera, and N&S	12 S, 244 W	9.9 S, 242.3 W 9.5 S, 242.7 W 11.5 S, 242.2 W	13±3 S, 244±3 W			G	yes	Major change in 1997
Pyerun Patera	55 S, 252 W			yes-same as Mithra?		no	no	
Pele	18 S, 256 W	18 S, 256 W	20±3 S, 255±3 W	yes		V,G	yes	Large, bright red deposits
Shakura Patera	24 N, 267 W			yes-same as Daedalus?		no	no	Very low albedo
Mithra Patera	59 S, 267 W			yes-same as Pyerun?		no	no	Red deposits
Svarog Patera	48 S, 268 W	53.9 S, 270 W	42±5 S, 269±5 W	yes		no	no	
Babbar Patera	39 S, 273 W		37±4 S, 283±8 W	yes		no	no	
Daedalus Patera	19 N, 275 W		18±3 N, 273±3 W	yes		no	yes	Red deposits
Viracocha Patera	62 S, 282 W			yes		no	no	
Ulgen Patera	40 S, 288 W		"merged" with Babbar?	yes		no	no	Very low albedo
Sengen Patera?	32 S, 304 W				9506J ?	no	yes	
Amaterasu Patera	38 N, 307 W		40±4 N, 309±4 W	yes		no	yes	Especially low albedo (usually)
Loki Patera	13 N, 309 W	10.8 N, 310.5 W	9±7 N, 309±7 W	yes	yes	V	yes	
Aten Patera	48 S, 311 W			yes		no	yes	Pele-type plume deposits, reddish
Mazda Catena	8 S, 314 W			yes		no	no	Red deposits
Nemea	80 S, 320 W			yes		no	no	
Ra Patera	8 S, 325 W					G	yes	Major brightening observed by HST in 1994 [Spencer 1987b]
Fuchi Patera	29 N, 328 W	maybe			9606G ?	no	no	Red deposits
Acala Fluctus	11 N, 336 W	10.7 N, 333.2 W		yes		G	yes	
Surt	46 N, 338 W				9606E ?	no	yes	Pele-type plume deposits, reddish
Creidne Patera	53 S, 344 W			yes		no	yes	
Tiermes Patera?	23 N, 351 W				9507A ?	no	no	
Euboea Fluctus?	45 S, 352 W				9606F ?	no	yes	Pele-type plume deposits, bright red
Fjorgynn Fluctus	12 N, 358 W				9606D ?	no	yes	

have treated the following multiple hot spot complexes as single volcanic centers: Kanehekili N&S, Isum N&S, and Pillan N&S. The reason is that most of the monitoring observations are from NIMS, and so far it has not been possible to resolve the multiple components seen by SSI in the NIMS observations. Treating these as single volcanic centers simplifies the analysis. A total of 14 hot spots were detected by both NIMS and SSI, often in observations taken during different orbits.

TABLE II
Identifications of Possibly Active Volcanic Centers

Volcanic center	Location of candidate surface feature	SSI hotspot?	Ground-observed hot spot?	Plume?	Surface Change?	Notes
Ruwa Patera	1 N, 3 W	1.4 N, 1.2 W		no	no	Faint bright spot in SSI G8 eclipse image
Unnamed		15.3 N, 4.7 W	9606D ?	no	no	Faint bright spot in SSI G8 eclipse image
Unnamed		2 S, 13 W		no	no	Faint bright spot in SSI G8 eclipse image
Unnamed		11.5 N, 13.3 W		no	no	
Unnamed		5.2 N, 24.1 W		no	no	Faint bright spot in SSI G8 eclipse image
Unnamed		10 S, 14 W	9606C ?	no	no	Faint bright spot in SSI G8 eclipse image
Unnamed		6 S, 19 W		no	no	Faint bright spot in SSI G8 eclipse image
Unnamed		1 N, 21 W		no	no	Faint bright spot in SSI G8 eclipse image
Unnamed		1 S, 23 W		no	no	Faint bright spot in SSI G8 eclipse image
Unnamed		9 S, 27 W		no	no	Faint bright spot in SSI G8 eclipse image
Unnamed		13.1 S, 22.8 W	9606C ?	no	no	Faint bright spot in SSI G8 eclipse image
Unnamed		16.5 S, 27.9 W	9606C ?	no	no	Faint bright spot in SSI G8 eclipse image
Unnamed (NE of Hi'iaka)	3 N, 76 W	3.8 N, 76.1 W		no	no	
"Poliahu"		no	yes	no	no	Reported at 22 ± 5 S, 79 ± 5 W by Goguen et al. [1988]
Catha Patera	53 S, 100 W	no		no	yes	
Arusha Patera	38 S, 101 W	no	9503A ?	no	yes	
Unnamed	42 N, 134 W	no		no	yes	Reddish materials
Unnamed	31 N, 146 W	no		no	yes	Large region of red deposits, coordinates are of center
Unnamed	21 N, 151 W	no		no	yes	
Unnamed		28.5 N, 189.4 W		no	no	
Unnamed	38 S, 291 W	no		no	no	Low albedo and bright red materials
Huo Shen Patera	15 S, 330 W	no		no	no	HST changes [Spencer et al. 1997] not confirmed by SSI
Unnamed		17.1 N, 332.9 W		no	no	
Unnamed		2 S, 352 W		no	no	Faint bright spot in SSI G8 eclipse image
Unnamed		4.8 N, 356.1 W		no	no	

Lack of detection of an SSI hot spot by NIMS is most likely due to the 50 times lower spatial resolution of NIMS or else the temporal variability of some hot spots. An example of the latter is probably the Reiden hot spot detected by SSI during orbit G1. NIMS did not observe the Reiden Patera region during G1. However, observations in several other orbits, at resolutions down to 122 km/pixel, have failed to detect this hot spot, but have detected all others shown in the same SSI G1 image. Since Reiden has not been observed as a hot spot by SSI in later orbits, it is likely that the activity there either stopped after the G1 observation by SSI or waned to levels below the sensitivity of either instrument. Alternatively, the SSI hot spot could have been spurious, although it is unlikely that noise would mimic the same shape as the smear ellipse.

Lack of detection of a NIMS hot spot by SSI is most likely due to the lack of a significant high temperature component (above 700 K), and hence of significant energy at 1 μm. These "cooler" hot spots include Hi'iaka, which was discovered from groundbased observations (Spencer *et al.* 1997a) and Malik, first seen as a hot spot by NIMS in orbit G1.

A total of 61 active volcanic centers are listed in Table I, plus two others that are hot spots identified from IRIS data, but have uncertainties large enough that more than one candidate site is listed (Mithra or Pyerun and Shakura or Daedalus). Table II lists an additional 25 sites that we consider likely to be active volcanic centers, but have yet to be confirmed. The activity at these sites is suggested by one or more of the following: (i) surface changes detected by comparing SSI and Voyager images, (ii) faint glow in an SSI eclipse image, which suggests a region of degassing or a faint hot spot, (iii) presence of reddish materials that are thought to be indicative of recent activity, (iv) possible identification of a hot spot detected by groundbased observations, or (v) possible identification of a site where changes were reported by observations from the Hubble Space Telescope (Spencer *et al.* 1997b).

The identification of volcanic centers on the surface corresponding to hot spots detected by groundbased observations can be problematic because of the large uncertainties associated with the positions of hot spots in these observations. Table III lists observations by Spencer *et al.* (1997a) during 1996 and 1997, with possible identifications based on data from Voyager and Galileo. Surface locations for two outbursts observed on Io between Voyager and Galileo (summarized by Spencer and Schneider 1996) have been obtained. An outburst observed on November 6, 1979 (Sinton 1980) has a location consistent with Surt, while an outburst detected on September 1, 1990 (Blaney *et al.* 1995) was most likely from Loki. Other reported outbursts have locations that are too uncertain for identification to be attempted, although Kanehekili would be consistent as the site of outbursts detected in 1986 and 1989 (Johnson *et al.* 1988, Veeder *et al.* 1994).

4. DISTRIBUTION OF HOT SPOTS ON THE SURFACE

The hot spots detected by NIMS and SSI, together with hot spots observed from the ground by Spencer *et al.* (1997a) during

TABLE III
1995 and 1996 Observations of Hot Spots by Spencer *et al.* (1997a)

NAME	FIRST SEEN	LAST SEEN	LATITUDE	LONGITUDE	COMMENTS AND POSSIBLE IDENTIFICATION (SURFACE FEATURES)
9503A	95/02/28	95/09/08	45 ± 7 S	98 ± 7 W	Outburst, Arusha Patera
9503B	95/03/16	95/04/24	?	0 ± 20 W	Bright event, position too uncertain for identification, but possibly Surt or same as 9507A
9507A	95/07/10	95/10/04	22 ± 5 N	351 ± 5 W	Bright event, Tiermes Patera
9508A	95/07/27	95/10/04	32 ± 8 N	20 ± 5 W	Bright event, Ukko Patera
Loki	95/08/19	96/02/06	13 ± 3 N	309 ± 3 W	Bright event, Loki Patera
9509A	95/09/04	96/10/04	45 ± 45 S	77 ± 45 W	Outburst, position too uncertain for identification
9510A	95/09/03	96/06/03	25 ± 15 N	220 ± 15 W	Bright event, Isum or Mulungu Patera
9606A	96/06/02	96/06/02	8 ± 10 S	41 ± 4 W	Janus Patera
Kanehekili	96/06/02	96/06/02	11 ± 8 S	34 ± 4 W	Kanehekili
9606C	96/06/02	96/06/02	25 ± 12 S	22 ± 12 W	SSI hot spot at (13S, 25W), or unnamed features at (10S, 14W) or (16S, 30W), or Uta Patera
9606D	96/06/02	96/06/02	19 ± 10 N	3 ± 5 W	SSI hot spot at (16N, 6W) or Fjorgynn Fluctus
9606E	96/06/02	96/06/02	50 ± 4 N	332 ± 6 W	Surt
9606F	96/06/02	96/06/02	39 ± 12 S	350 ± 12 W	Euboea Fluctus
9606G	96/06/02	96/06/02	20 ± 12 N	326 ± 6 W	Fuchi Patera
9606H	96/06/02	96/06/02	0 ± 30	316 ± 6 W	Position too uncertain for identification
Loki	96/06/02	96/06/02	11 ± 5 N	307 ± 4 W	Loki Patera
9606J	96/06/02	96/06/02	36 ± 8 S	307 ± 6 W	Sengen Patera
9606K	96/06/02	96/06/02	30 ± 20 S	300 ± 6 W	Position too uncertain for identification
9608A	96/08/23	96/09/15	2 ± 10 N	16 ± 3 W	Bright event, Karei Patera
9610A	96/10/01	96/10/08	70 ± 15 N	35 ± 15 W	Bright event, N. Polar region
Loki	97/02/20	-	13 ± 3 N	309 ± 3 W	Bright event, Loki Patera
9706A	97/05/31	97/06/14	?	345 ± 90 W	Bright event, position too uncertain for identification

Note. The hot spots which were *not* detected by either NIMS or SSI are 9503A (Arusha?), 9507A (Tiermes?), 9508A (Ukko?), 9606E (Surt?), 9606F (Euboea?), 9606J (Sengen?), and 9610A (N, Polar region). SSI may have seen hot spots 9606G (Fuchi?) and 9608A (Karei?), but detection is still uncertain. The positions of hot spots 9503B, 9509A, 9606H, 9606K, and 9706A are too uncertain for correlation with Galileo or Voyager data to be possible. Other hot spots may correspond to those detected by Galileo or Voyager, though in some cases the position is too uncertain for a definite identification to be made.

1995 and 1996, are shown superimposed on a global mosaic of SSI images of Io (Fig. 1). The "Galileo-era" view of the distribution of hot spots on Io can be compared with the "Voyager-era" view, on which hot spots detected from IRIS data are plotted. It is clear that many more hot spots are present on Io than was known from analysis of the limited-coverage Voyager IRIS data, which revealed 22 hot spots over about 30% of Io's surface. We note that Galileo has not detected activity at 10 of these 22 hot spots (Nusku, Mbali, Uta, Pyerun/Mithra, Viracocha, Ulgen, Aten, Mazda, Nemea, and Creidne). SSI detected surface changes at Aten and Creidne, perhaps due to activity occurring between Voyager and Galileo observations. The hot spot Ulgen may have been detected by NIMS, but even in the current highest resolution observations by NIMS, the pixel size is still too large to enable us to confidently distinguish it from the Babbar hot spot.

The locations of active volcanic centers listed in Table I can be used to search for possible correlations with latitude, longitude, or topography, which may have important implications for the mechanism of heat dissipation on Io. The active volcanic centers used for the following analysis are from Table I. Since two Voyager hot spots had uncertain identifications (Shakura/Daedalus and Mithra/Pyerun), we have included both possibilities in our analysis. Daedalus is known to be a hot spot from Galileo data, but Shakura and either Mithra or Pyerun may be spurious data points.

4.1. Distribution with Latitude and Longitude

The distribution of active volcanic centers (from Table I) shows no obvious correlation with latitude or longitude, as indicated in the histograms in Fig. 2. This agrees with McEwen's (1995) earlier study from Voyager data. Carr *et al.* (1998) plotted the distribution of calderas and other surface features interpreted as volcanic centers and also concluded that the large-scale distribution was uniform, except for an apparently somewhat lower density at high latitudes. We note from Fig. 2 that there is an apparently lower concentration of active volcanic centers between latitudes 20 S and 30 S, and 0 to 10 N, but the present data are not sufficient to establish whether these departures from an uniform distribution are significant.

A factor that needs to be taken into account when considering the Galileo data is the spacecraft viewing geometry. Hot spots at latitudes over 45° are viewed by Galileo at lower spatial resolutions than the equatorial regions and are therefore likely to be harder to detect (the subspacecraft point of all NIMS observations and SSI eclipse observations is near the equator). In addition to lower resolution, there is the possible effect of topography. For example, a lava lake in a caldera will be increasingly obscured by the caldera wall at higher emission angles. The obscuration will depend on the depth and the diameter of the caldera, and the emission angle. A more subtle topographic effect involves molten material at the bottom of incandescent cracks. Hot spots surrounded by extensive hot lava flows, or erupting high fire fountains, could be detected at higher emission angles.

In many NIMS observations, we have noticed that hot spots can be detected near Io's limb, indicating that the effect of viewing geometry (emission angle) may not be substantial. The emission angle for each pixel is defined as the angle between the observer (spacecraft) and the normal to a planitodetic surface. We have examined the viewing geometry effect in Fig. 3, where data

from five NIMS observations (between orbits G2 and E4) were plotted. These observations were all taken at spatial resolutions from 122 to 350 km/pixel. They were all taken in reflected sunlight, therefore we have estimated the 5-μm flux for individual hot spots by subtracting the 5-μm flux of a nearby "cold" pixel. While this is a crude method to obtain the flux for hot spots, because of possible differences in albedo between the hot spot and the "cold" pixel (which may still contain a small amount of thermal energy), it is satisfactory for assessing the effect of emission angle (and thus viewing geometry) on the brightness of hot spots in general. The effect of emission angle is partly illustrated by the changes in the flux of Prometheus and Pele, though some temporal variation in the flux may also have occurred. While emission angle clearly has an effect, Fig. 3 also illustrates that the hot spots detected by NIMS are sufficiently bright that they can still be detected at high emission angles. There is no clear correlation between the number of hot spots detected by NIMS and emission angle.

We consider that it is unlikely that there is a large number of hot spots undetected by NIMS at high latitudes *of comparable brightness* to the hot spots shown in Fig. 3. However, the detection of the hottest material by both NIMS and SSI is probably more sensitive to the effect of small-scale topography (and hence emission angle). The hottest material is more likely to be located inside cracks rather than on the flow surface, and thus be obscured at high emission angles.

The distribution of active volcanic centers with longitude (Fig. 2) also appears uniform when all the hot spot detections by the different instruments are combined. NIMS observations have higher spatial resolution on the anti-jovian hemisphere, and this is reflected in the relatively low number of hot spots detected between longitudes of about 320 W and 30 W. SSI imaged these longitudes in eclipse several times during the Galileo tour (McEwen *et al.* 1998a), and Voyager IRIS obtained more complete coverage on the Jupiter-facing hemisphere, which is also the preferred hemisphere for groundbased observations. The complementary coverage of NIMS, SSI, and IRIS gives us confidence that we have a reasonable sample of the number of hot spots present at all longitudes. It is, however, possible that additional hot spots with temperatures below the SSI limit of 700 K are present on the Jupiter-facing hemisphere, and have not been detected by NIMS due to poor spatial resolution at those longitudes. A possible departure from the apparently uniform distribution in longitude may be implied by the detection by SSI of a field of about 26 bright spots near the subjovian point (at $0^\circ \pm 15^\circ$ latitude, $0^\circ \pm 30^\circ$ longitude, McEwen *et al.* 1998a). It is not clear from the current SSI images whether these are hot spots, excited gases concentrated near vents, or both. McEwen *et al.* (1998a) also reported a diffuse glow over this region, and over a region of similar size near the anti-jovian point which may suggest that a similar field of bright spots is present there. NIMS has not detected a concentration of hot spots near the anti-jovian point, even though the spatial resolution of NIMS is highest on that hemisphere. We cannot rule out that hot vents may exist near the anti-jovian point that are simply too small in area to be identified with the available measurements.

4.2. Distribution of Active Volcanic Centers and Relation to Tidal Heating Models

Hot spots are manifestations of Io's mechanism of internal heating and heat transfer. Most of Io's heat flow is radiated at wavelengths longer than 10 μm (e.g., Veeder *et al.* 1994), beyond the range of what NIMS and SSI can observe. However, the distribution of hot spots on the surface seen by the two instruments is useful for constraining models of internal heating. If we assume that these hot spots represent the major pathways of magma to Io's surface, then they would reflect the distribution of the total heat flow.

Two major models have been proposed for the dissipation of tidal heating in Io. Both models assume that convection is the main mode of heat transfer within Io, but differ on where the tidal heating predominantly occurs (Segatz *et al.* 1988, Ross *et al.* 1990, Gaskell *et al.* 1988). If heating occurs mainly in an asthenosphere about 100 km thick, convection should occur globally, with centers of upwelling and downwelling separated by a few hundred kilometers. In the second model, tidal heating occurs in the deep mantle and results in larger-scale convection, perhaps with a relatively small number of mantle plumes spaced widely apart. The deep mantle model predicts greater heat dissipation (and higher concentration of hot spots) toward the poles. It is likely that some tidal heating does occur both in the deep mantle and in the asthenosphere; thus a combination of the two models, such as the $2/3$ asthenosphere and $1/3$ mantle heating model (Ross *et al.* 1990, Schubert *et al.* 1998), may be the most realistic scenario. In this paper, we consider only the two end-member models, as the difference in the heat flow patterns at the surface predicted by these two models is the most pronounced and may be reflected in the distribution of volcanic centers.

An earlier attempt to use spacecraft data to distinguish between these models was made by Gaskell *et al.* (1988), using the shape and large-scale topography of Io determined from Voyager 1 images. They proposed that the broad topographic swells suggested in the global topography could be due to isostatic responses to thermal changes in the lithosphere-asthenosphere system. In the simplest picture, increasing the heat flow converts the basal lithosphere into lower density asthenosphere, resulting in isostatic uplift. In this scenario, the global pattern of basins and swells would suggest that tidal dissipation occurs mostly in the asthenosphere. McEwen (1995) found no correlation between Voyager-detected hot spots and topography, but argued that the distribution of SO_2-rich areas on the surface supported the asthenosphere model.

We can use the combined Galileo, Voyager, and other data on active volcanic centers on Io (Table I) to reexamine the relation between active volcanic centers and topography. The distribution of active volcanic centers from Table I is plotted on Gaskell *et al.*'s topographic map in Fig. 4a. A plot of the number of active volcanic centers relative to the map's elevations and areas

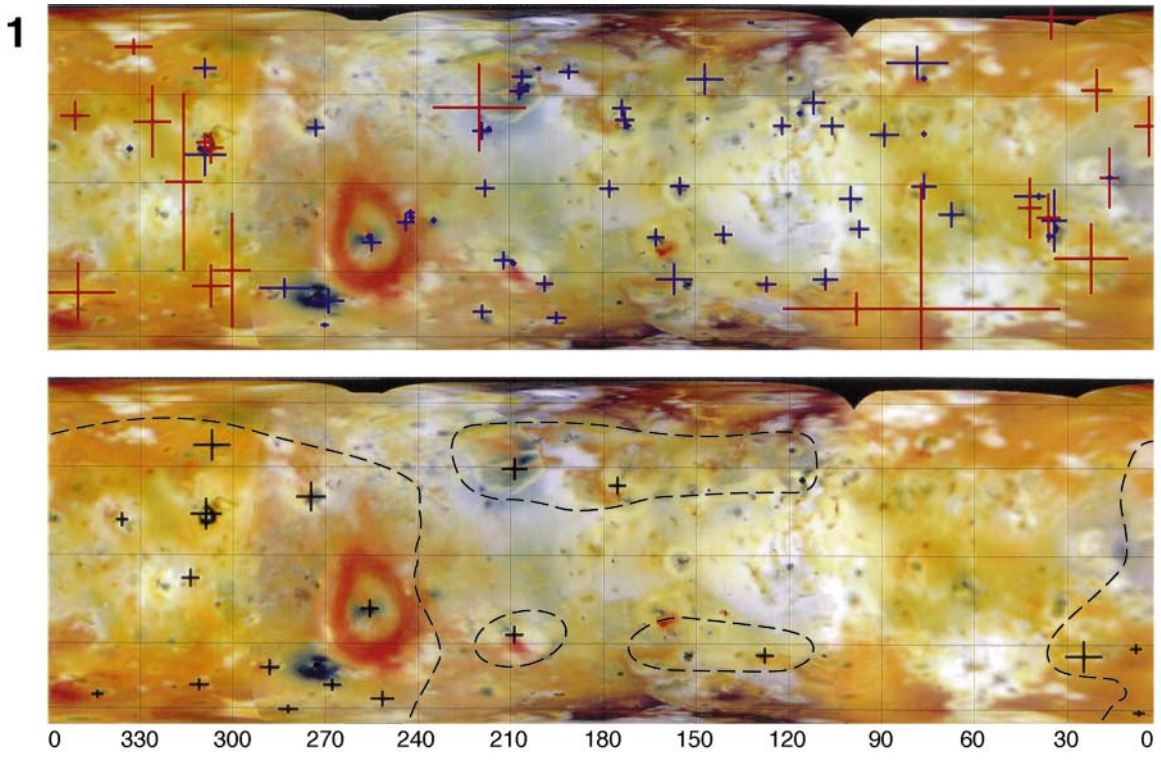
1
0 330 300 270 240 210 180 150 120 90 60 30 0

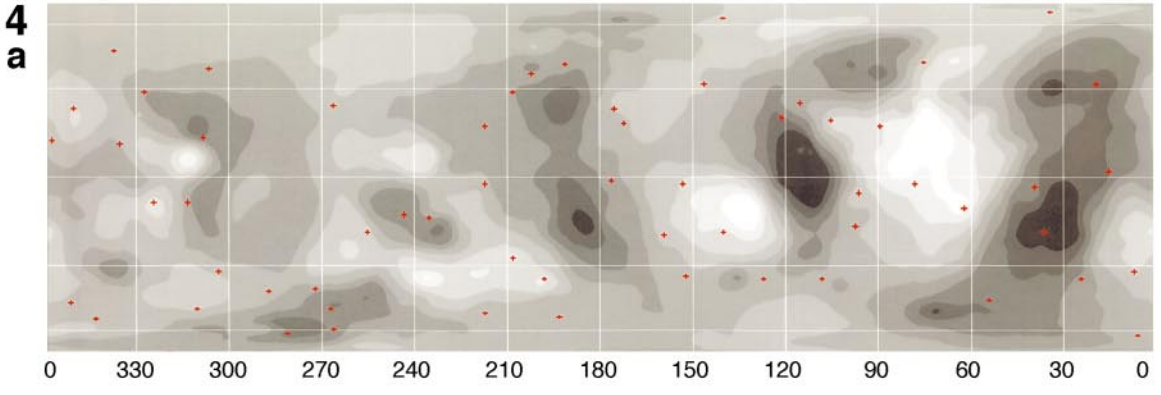
4
a
0 330 300 270 240 210 180 150 120 90 60 30 0

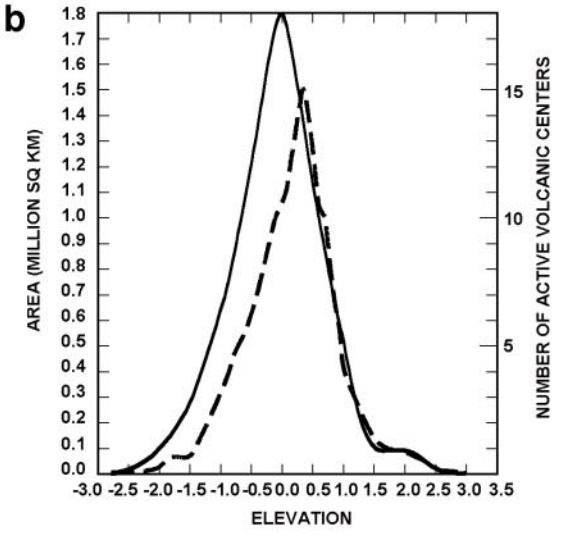
b
AREA (MILLION SQ KM)
NUMBER OF ACTIVE VOLCANIC CENTERS
ELEVATION
-3.0 -2.5 -2.0 -1.5 -1.0 -0.5 0.0 0.5 1.0 1.5 2.0 2.5 3.0 3.5

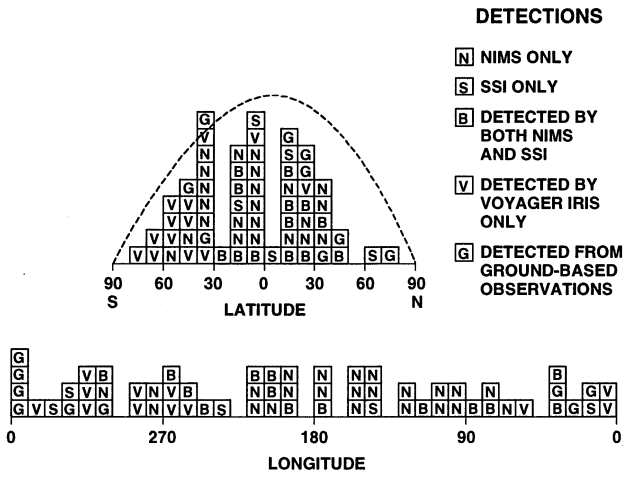

FIG. 2. Distribution of active volcanic centers (from Table I) with latitude (above) and longitude (below). The dashed line represents the expected result for a uniform areal distribution of hot spots with latitude. The higher number of Voyager IRIS hot spots at high latitudes on the southern hemisphere than on the northern reflects the geometry of the Voyager flyby.

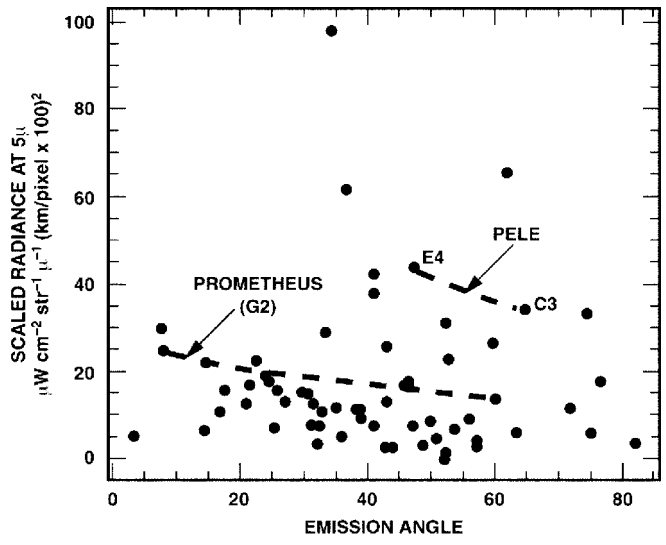

FIG. 3. Hot spots detected during five NIMS observations between orbits G2 and E4. All observations were taken in reflected sunlight. The 5-μm flux for individual hot spots is estimated by subtracting the 5-μm flux from a nearby "cold" pixel. The flux is plotted against the emission angle for each hot spot in order to assess the effect of viewing geometry. There is no clear correlation between number of hot spots detected and emission angle. The effect of emission angle is partly illustrated by the changes in the 5-μm brightness of Prometheus and Pele, though it is likely that actual changes in the flux also took place.

(Fig. 4b) fails to show any significant correlation between the locations of active volcanic centers and topography. We note, however, that the plot in Fig. 4b is skewed toward lower elevations, implying a possible (but not statistically significant from the available data) higher concentration of active volcanic centers at lower elevations. This is the opposite of what might be expected from the isostatic uplift model.

More recent results on Io's topography from Thomas *et al.* (1998), obtained from limb measurements made by Galileo SSI, show some disagreement with Gaskell *et al.*'s map. For example, Thomas *et al.* (1998) did not confirm the pattern of longitudinal swells inferred by Gaskell *et al.* (1988) and Ross *et al.* (1990), which was used to support the asthenosphere tidal dissipation model. It is clear that the relation between locations of active volcanic centers and topography needs to be reexamined once improved global topography becomes available.

The spatial separation between active volcanic centers may help to differentiate between the asthenosphere and deep mantle models (McEwen *et al.* 1998a). In the asthenosphere model, hot spots are expected to be uniformly distributed on the surface, separated at intervals of several hundred kilometers, perhaps with a preference for low latitudes. In the deep-mantle model, the centers of upwelling are further apart, and we might expect to find concentrations of hot spots in regions that would be widely separated from one another. Our data from Table I shows that the spacing between major hot spots ranges from about 150 km to about 700 km, with most hot spots being separated by about 200–400 km. The distribution is therefore more consistent with the asthenosphere model, in agreement with the conclusions by McEwen *et al.* (1998a) and Carr *et al.* (1998).

We can examine the overall spatial distribution of active volcanic centers on the surface in relation to the predicted heat flow surface patterns of the two major models. According to Ross *et al.* (1990), "although heat transfer processes will 'smear' the interior heating distributions by the time the thermal energy appears at the surface, the signatures should be evident in the surface heat flow and the location of volcanoes and hot spots." We can test this prediction, in part, by plotting the distribution of active volcanic centers over the heat flow patterns (Fig. 5) predicted by the two major models (from Ross *et al.* 1990). While the locations of the active volcanic centers do not appear to correlate well with the predicted heat flow patterns from either model, it is more consistent with the asthenospheric model because of the apparently uniform distribution of active volcanic centers with longitude and latitude.

FIG. 1. (Top) Distribution of hot spots on Io, shown on a global mosaic made from Galileo SSI images. Hot spots marked in dark blue were detected by Galileo SSI and NIMS; hot spots marked in red were detected by groundbased telescopes. (Bottom) Distribution of hot spots detected by Voyager IRIS, which had only a limited view of the surface of Io. The approximate coverage of Voyager IRIS observations is shown by the dashed lines (from Pearl and Sinton 1982).

FIG. 4. (a) Distribution of active volcanic centers (from Table I) plotted on the topographic map from Gaskell *et al.* (1988). The contours are in 0.5-km intervals, from −2 km (darkest) to +2 km (lightest). (b) Comparison of distribution of active volcanic centers and area with elevation. Dashed line: relationship between area and elevation, from Gaskell *et al.* (1988). Solid line: distribution of active volcanic centers with elevation.

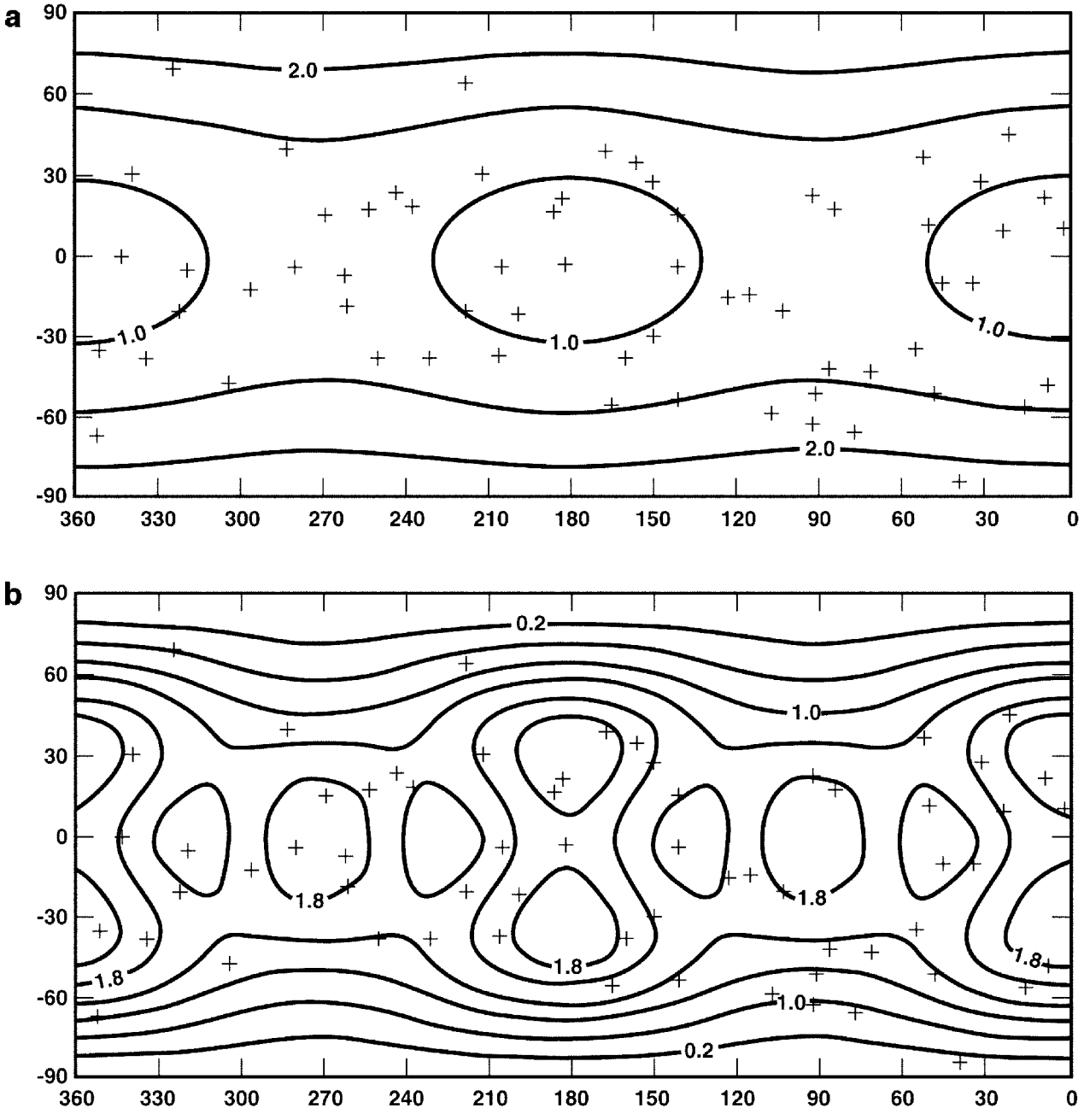

FIG. 5. Plots of distribution of active volcanic centers (from Table I) plotted over the heat flow patterns predicted by Ross *et al.* (1990). (a) Deep-mantle model. (b) Asthenosphere model. Heat flow contours in watts per meter squared.

Although the global distribution and typical separations of active volcanic centers on Io are consistent with the asthenosphere model, measurements of volcanic heat flow from individual hot spots at a range of wavelengths are needed for more conclusive evidence. Volcanic heat flow has been measured by NIMS in the range 0.7 to 5.2 μm. Thermal maps made from NIMS nightside data, using the method of Smythe *et al.* (1997, 1999), will be important for determining patterns of volcanic heat flow. To the extent that the volcanic heat flow at these wavelengths is correlated with total surface heat flow, these measurements may provide a stronger basis for discriminating between tidal dissipation models than the distribution of active volcanic centers.

5. CORRELATION BETWEEN ACTIVE VOLCANIC CENTERS AND SURFACE FEATURES

The location of enhanced thermal emission detected by both NIMS and SSI can be correlated with features on the surface

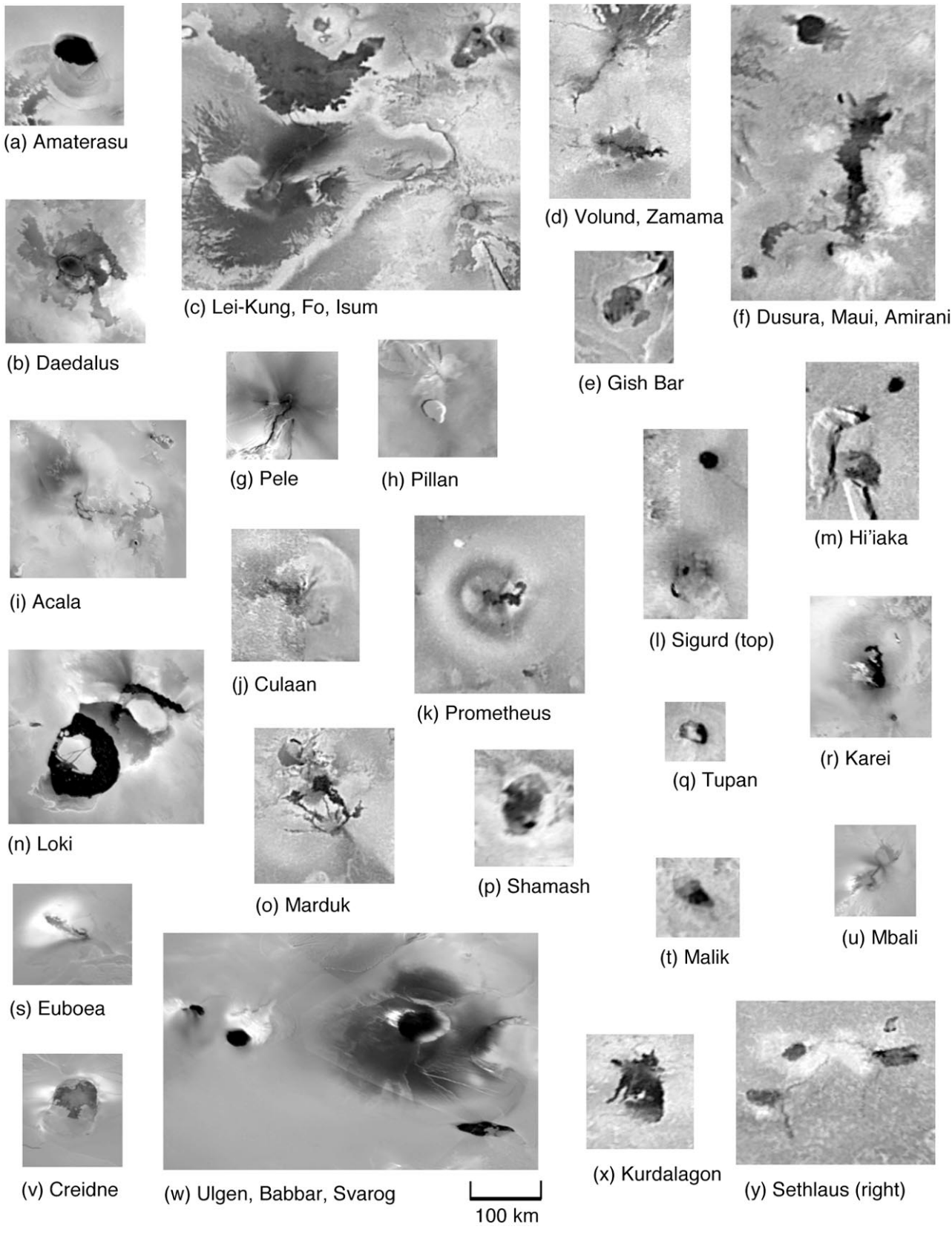

FIG. 6. Surface features associated with active volcanic centers. Images of Loki, Amaterasu, Babbar, Mbali, Karei, Daedalus, Pele, Pillan, Creidne, Acala, and Euboea are from Voyager, others are from Galileo SSI. Scale is 2 km/pixel in all cases. All are simple cylindrical projection, clear filter images.

7

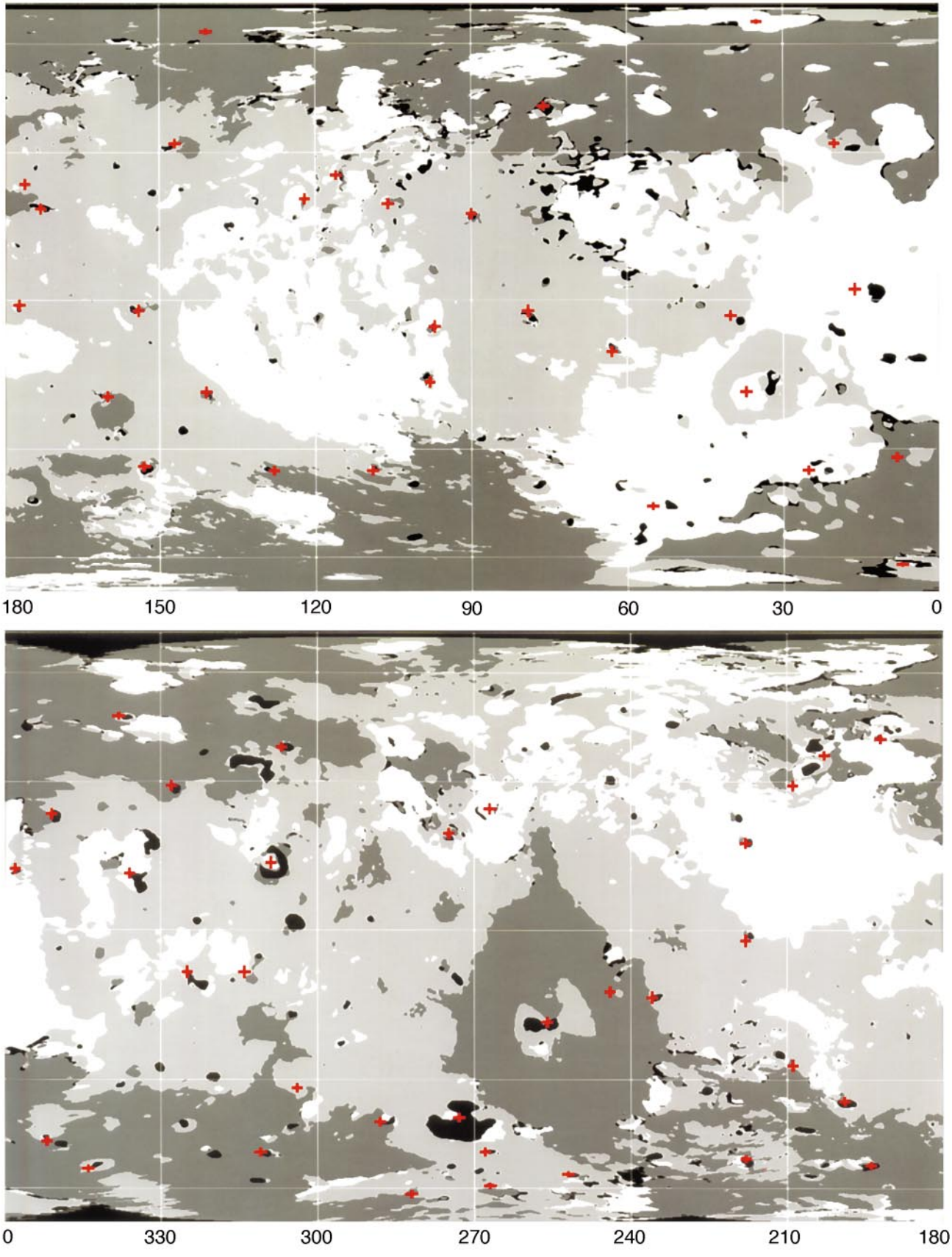

imaged by SSI. Tables I and II show the correlation between active volcanic centers and features on the surface that we consider to be candidate vent regions. The latitudes and longitudes given are approximately those of the center of the surface features. The most common surface feature is a patera (usually a caldera), but other features include flucti (flows) and fissure-like features. A sample of surface features is shown in Fig. 6.

Io presents a variety of surface colors, which are described in detail by McEwen *et al.* (1998a) and Geissler *et al.* (1999). The relation between the active volcanic centers (Table I) and surface colors is shown in Fig. 7, a map of the four major color units on Io. Red and orange materials dominate the dark polar regions of Io and are found at lower latitudes in isolated bright deposits; yellow and yellow–green materials, and white and gray materials, are mostly found at low latitudes; and low-albedo materials occur mostly in many small spots marking the locations of active calderas (Geissler *et al.* 1999). SSI results (McEwen *et al.* 1998a, Geissler *et al.* 1999) have confirmed the suggestion from Voyager observations (Pearl and Sinton 1982, McEwen 1995) that hot spots are associated with low-albedo materials. Note that the map in Fig. 7 does not show all of the low-albedo features, since some are too small to be shown at the scale of the map.

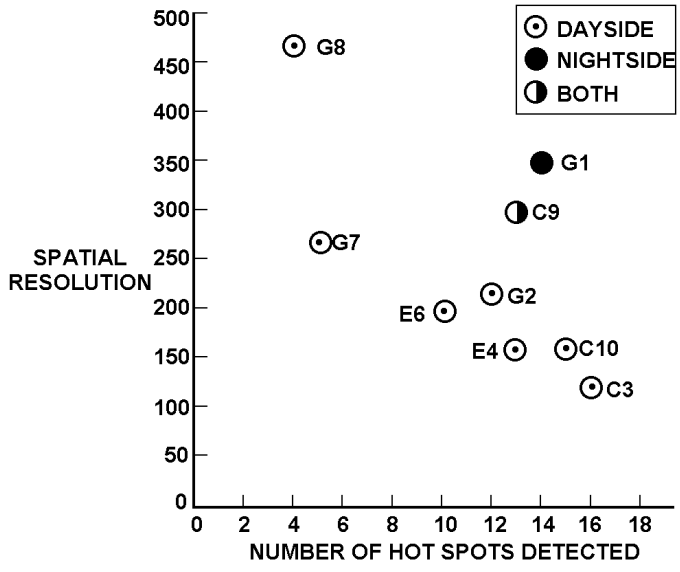

FIG. 8. Plot showing NIMS spatial resolution of the closest approach observation in each orbit against the number of hot spots detected in each of those observations.

5.1. Red Deposits

Red deposits are commonly associated with hot spots (Spencer *et al.* 1997b, McEwen *et al.* 1998a, Geissler *et al.* 1999). Most regions that present red materials have been identified as hot spots or regions of surface changes (Geissler *et al.* 1999). The red deposits may be fallout from plumes, possibly fine droplets that were rapidly quenched, as discussed by Moses and Nash (1991). They appear to fade with time and their spectral properties (as revealed by HST and Galileo SSI observations) are consistent with metastable short-chain S_3/S_4 molecules mixed with elemental sulfur or other sulfurous materials (see summary by Spencer *et al.* 1997b). NIMS observations obtained up to now cannot spatially resolve the red deposits except for those in the ring surrounding Pele. Carlson *et al.* (1997) reported the presence of a 1.25-μm absorption feature, which may be due to iron-containing minerals, nearly everywhere on Io's surface, but not on the red ring surrounding Pele. Carlson *et al.* suggested that the red deposits, which may be sulfur from plume fallout, could be covering the iron-containing deposits on the surface.

The inventory of hot spots and plume sites presented in Table I allows us to further investigate the correlation between red materials, hot spots, and plume sites. In Table I, we have identified 59 hot spots from Voyager, Galileo, and groundbased data. Thirty-nine percent of these hot spots have red deposits associated with them (23/59). If red deposits are indeed the result of plume activity, this may possibly reflect a lower limit of how often plume and hot spot activity are associated.

Plume activity is perhaps only found at hot spots, but the reverse is probably not true. Plumes have not been detected at most hot spots, though they could occur sporadically. Long time intervals between plume activity, or very short durations, would make detection difficult. There are only two known plume sites where hot spots have so far not been detected: Ra, observed by SSI in G1, and Masubi, observed by Voyager. The lack of detection of a hot spot at Masubi by Voyager may well have been due to the very poor resolution of IRIS at that location. Up to orbit C10, no plume or hot spot had been detected at Masubi by Galileo, though more recent results indicate the presence of a hot spot and new plume deposit at Masubi. No hot spot has been detected at Ra by either NIMS or SSI, even though both instruments have viewed the location in several observations at different geometries. The lack of detection of a hot spot could be due to temporal variability, to relatively cool temperatures making it unlikely to be detected by SSI, and to the poor spatial resolution of NIMS at the longitude of Ra (325 W). Red deposits are not seen by Galileo SSI at either Masubi or Ra.

How well do plumes and red deposits correlate? Plumes have only been observed by SSI at 5 (6, if we include the marginal

FIG. 7. Active volcanic centers (from Table I) plotted on map of Io's major color units (from Geissler *et al.* 1998). Black corresponds to low-albedo areas, dark gray to red/orange areas, light gray to yellow/green areas, and white to white/light gray areas. The imaging data used to make these maps have poorer resolution (and positional errors) in the subjovian hemisphere, centered on 0° longitude. This uncertainty is probably responsible for hot spots between 0° and 60° being consistently to the left of low-albedo areas.

TABLE IV
Detection of Activity at Io's Hot Spots by Galileo

Hot spot	Voyager	Ground based?	G1 SSI	G1 NIMS	G2 NIMS	C3 NIMS	E4 SSI	E4 NIMS	E6 SSI	E6 NIMS	G7 SSI	G7 NIMS	G8 SSI	G8 NIMS	C9 SSI	C9 NIMS	C10 SSI	C10 NIMS
Kanehekili		yes					yes				yes	yes	yes			yes	yes	yes
Janus		yes		yes			yes				yes	no	yes			no	yes	yes
Shamshu				no	no	no	no				no	no	no			no	no	yes
Zal				yes	no	no	no				yes	no	yes	no		yes	no	yes
Hi'iaka		yes		yes	no	yes	no				no	yes	no	yes		yes	no	yes
Gish Bar				yes	no	yes	yes			no	no	no	no	no		no	no	yes
Sigurd				yes	no	yes	no			no	no	no	no	no		yes	no	yes
S. Sigurd				no	no	no	no			no	no	no	no	no		no	no	yes
Monan				yes	yes	yes	no			no	no	no	no	no		no	no	yes
Altjirra	?			yes	no	yes	no			yes	no	no	no	no		yes	no	yes
Amirani	yes			yes	yes	yes	no			yes	no	yes	yes	yes		yes	yes	yes
Maui	?			yes	yes	yes	no			?	no	?	no	?		?	no	?
Malik	yes			yes	yes	yes				yes	no		no	yes		yes	no	yes
N. Polar				no	no	no				no	yes		no	no		no	no	no
Tupan				yes	yes	yes				yes	no		no	no		yes	no	yes
9606W			no	yes	no	yes				no	no	no	no	no		no	no	?
Shamash	?		no	yes	no	no				no		no	no	no		yes	no	yes
Prometheus			no	yes	yes	yes				yes		yes	no	no		yes	no	yes
Culann			no	yes	yes	yes				no		no	no	yes		yes	no	yes
Zamama			yes	yes	yes	yes		yes		no		no		no		no	no	yes
Volund	yes		no	?	?	yes		?		no		no		no		no	no	yes
Aidne			no	yes	yes	yes		yes		no		no		no		no	no	yes
Fo			yes		no	yes		no		yes		no		no	no	no	no	no
Sethalus			no		no	yes		yes		yes		no		no	no	no	no	yes
Rata			no		no	yes		yes		yes		no		no	no	no	no	no
Lei-Kung			no		no	yes		no		no		no		no	no	no	no	no
Isum-N,S	yes	?	yes		yes	yes		yes	no	yes		yes		yes	no	yes	no	yes
Marduk	yes		yes		yes	yes		yes	no	yes		yes		yes	yes	yes	no	yes
Kurdalagon			no		no	yes		yes	no	yes		no		no	no	no	no	no
9611A			no		no	yes		yes	no	yes		no		no	no	no	no	no
Mulungu		?	yes		yes	yes		yes	no	yes		yes		yes	no	yes	no	yes
Reiden			yes		no	no		no	no	no		no		no	no	no	no	no
Pillan			no		yes	yes		yes	no	yes		yes		yes	yes	yes	yes	yes
Pele	yes		yes		yes	yes		yes	yes	yes		yes		yes	yes	yes	yes	yes
Svarog	yes		no		no	no		no	no	no		yes		?	yes	no	no	no
Babbar	yes		no		yes	yes		yes	no	yes		yes		yes	no	yes	no	no
Daedalus	yes		no		no	no		yes	no	yes		no		no	no	no	no	no
Amaterasu	yes		no		?		no	?	no	yes		yes		yes	no	?	no	?
Loki	yes	yes	no		yes		no	yes	yes	yes		yes		yes	no	yes	no	yes
Acala	yes						no		no	no	no				yes	no	no	no

Note. Blank = no observation by Galileo, ? = possible detection by Voyager or by NIMS. The marginal detection of Karei by SSI is not included.

identification of a plume at Culann) of the 23 hot spots associated with red deposits (22 or 26%), but this is a higher occurrence than plumes observed by Galileo at hot spots not associated with red deposits (3 plumes detected at 36 hot spots, or 8%). We do not include Voyager-observed plumes because red deposits cannot be identified reliably from Voyager ISS data (Geissler *et al.* 1999). While it can be argued that red deposits are the result of plume activity, and that plumes were at one time present at the active volcanic centers now showing red deposits, it is clear that at least a few plumes have not produced red deposits. Bright white deposits surround some plumes sites and may be produced by plumes containing pure SO_2. Diffuse dark deposits found at other sites may represent silicates in the plume.

Can we constrain the lifetime of red deposits using Galileo data? If we postulate that red deposits, plume activity, and hot spots are associated, we can use the Galileo NIMS and SSI data to further constrain the lifetime of the red deposits. One striking example is Tohil Patera (at 26S, 158W), which is surrounded by red deposits. SSI has not detected a hot spot, plume, or surface change at Tohil during the Galileo mission. Voyager IRIS also did not detect a hot spot at Tohil, but this could easily be due to the poor spatial resolution of IRIS over this hemisphere. NIMS has observed this region at least once per orbit (except orbit E4), detecting hot spots at regions nearby (such as Shamash and Culann) but not at Tohil. While it cannot be ruled out that Tohil is a faint hot spot below the resolution limit of both NIMS and SSI, it can safely be said that Tohil has not had activity at a comparable level to that of other hot spots in the region since Galileo begun observing in June 1996. It has possibly not been active at all during this time. The lack of activity would imply that the lifetime of the red deposits can be at least 18 months.

5.2. White Deposits

Active volcanic centers are generally anti-correlated with large areas of bright white deposits. As Fig. 7 shows, the surface of Io has large regions that are predominantly white and mostly occur at low latitudes. These regions were first seen on Voyager images

TABLE V
Detection of Persistently Active Hot Spots (Orbits G1–C10)

Hot Spot	Voyager?	Ground?	Galileo N (Detected)	N (Observed)	Ratio
Pele	Yes	Yes	9	9	100%
Mulungu	?		9	9	100%
Marduk	Yes		9	9	100%
Isum	Yes	?	9	9	100%
Amirani	Yes		8	8	100%
Hi'iaka		Yes	6	6	100%
Kanehekili		Yes	5	5	100%
Pillan			8	9	89%
Loki	Yes	Yes	7	8	88%
Malik	Yes		7	8	88%
Prometheus	plume only		7	8	88%
Janus		Yes	5	6	83%
Zal			5	6	83%
Tupan			6	8	75%
Culann			6	8	75%
Altjirra	?		5	9	56%
Zamama			5	9	56%
Aidne			5	9	56%
Gish Bar			4	9	44%
Sigurd			4	9	44%
Monan			4	9	44%
Shamash ?			3	8	38%

Note. Activity at these 22 hot spots was detected on a timescale greater than 1 year. Lack of detection at particular orbits may be the result of temporary waning of activity or observational constraints.

and interpreted by Smith *et al.* (1979) to be rich in SO_2 frost or ice. NIMS spectral mapping from an observation that included the bright white equatorial regions of Colchis Regio (centered at about 210 W) and part of Bosphorus Regio (centered at about 120 W) showed that these areas have extensive snowfields of SO_2 with larger particles (>250 μm in diameter) beneath smaller particles, while the pervasive covering of SO_2 elsewhere has smaller characteristic grain sizes (Carlson *et al.* 1997).

The identification of higher concentrations of SO_2 frost in the bright white areas, which are anti-correlated with hot spots, is consistent with these areas being colder than the surrounding regions where hot spots are located. Volcanic activity supplies SO_2, which condenses in regional cold traps that sustain SO_2 snowfields, as discussed by Fanale *et al.* (1982) and Kerton *et al.* (1996). A particularly good example of the anti-correlation between hot spots and bright white areas is Bosphorus Regio. Lopes-Gautier *et al.* (1997a) presented a NIMS 5-μm map from a nightside observation of Bosphorus Regio. The map shows that pixels located in the center of Bosphorus Regio (corresponding to the bright white area) have no detectable thermal signal, while the pixels surrounding Bosphorus Regio show significant thermal signal and form a hot spot "ring of fire."

While the anti-correlation between hot spots and cold SO_2 snowfields (bright white areas) is to be expected, it is not clear why the bright white areas occur geographically where they do. Voyager data suggest that SO_2 is concentrated in equatorial topographic basins (McEwen 1995). However, as discussed previously, topography from SSI data has not confirmed the existence of these basins (Thomas *et al.* 1998).

6. HOT SPOT ACTIVITY

A summary of Galileo's detections of hot spot activity in different orbits is given in Table IV. Lack of detection of a hot spot by SSI or NIMS does not necessarily mean that the hot spot was not active at the time of the observation, but rather that the level of activity was below the detection limits for the instruments. This could mean temperatures too low, or spatial extent too small, to be detectable by either instrument.

It is clear that the spatial resolution of NIMS observations is a strong factor in whether hot spots can be detected. Another factor is whether the observation is of Io's dayside or nightside, as the solar component masks faint hot spots. Figure 8 shows a plot of the highest resolution NIMS observation in each orbit against the number of hot spots detected in each of those observations. NIMS detected fewer hot spots in orbits G7 and G8, where the range to Io was largest, than in other orbits, particularly C3, the closest approach to Io during the G1–C10 period. Therefore, the gaps in hot spot detection by NIMS shown in Table IV may not reflect halts in activity, but activity below the detection at the NIMS spatial resolutions at each particular orbit. More hot spot activity may be detected when pixel-by-pixel thermal maps of NIMS observation are completed.

The combination of NIMS, SSI, groundbased, and Voyager data show that some hot spots appear to be persistently active,

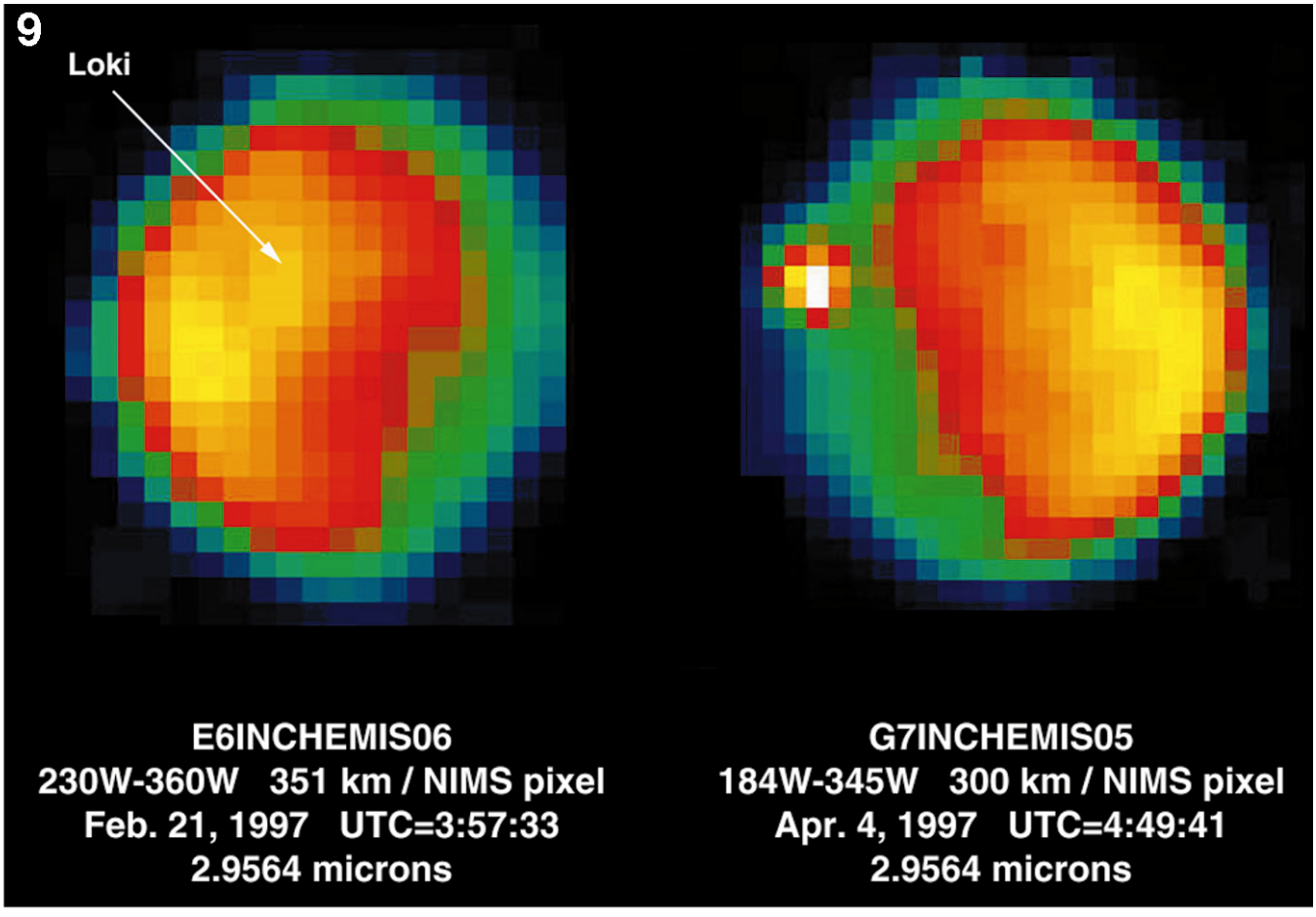
9
Loki
E6INCHEMIS06
230W-360W 351 km / NIMS pixel
Feb. 21, 1997 UTC=3:57:33
2.9564 microns
G7INCHEMIS05
184W-345W 300 km / NIMS pixel
Apr. 4, 1997 UTC=4:49:41
2.9564 microns

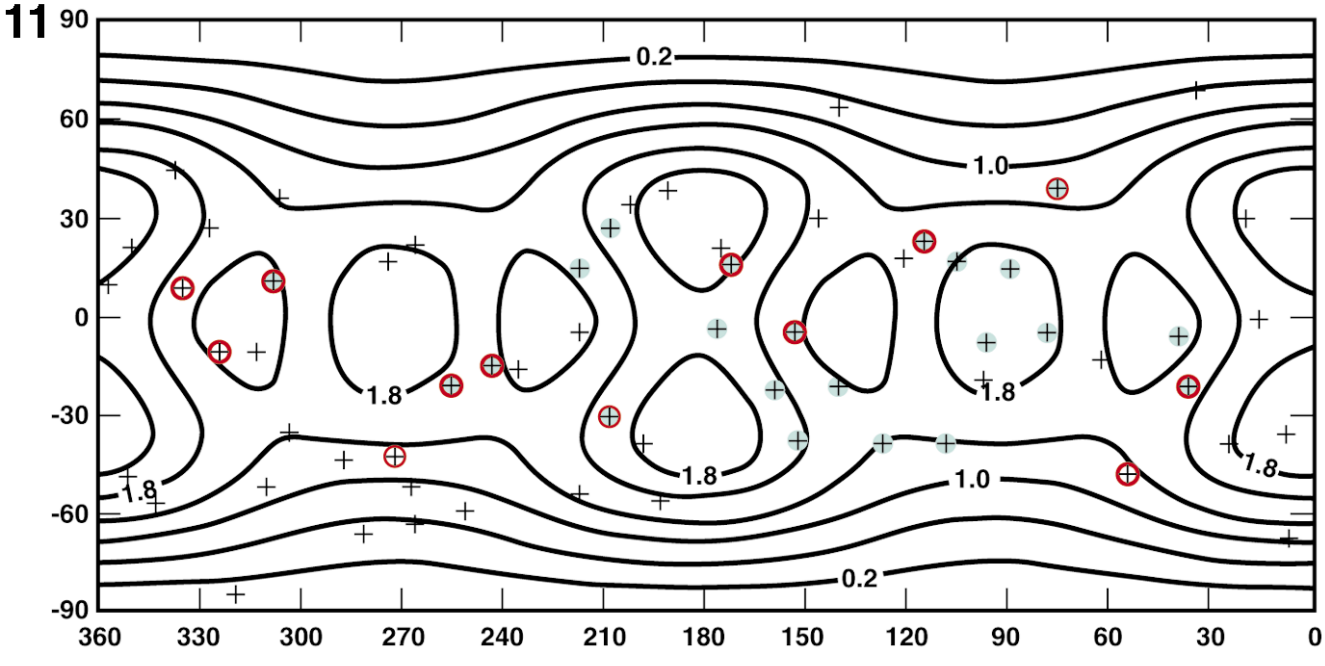
11
90
60
30
0
-30
-60
-90
360
330
300
270
240
210
180
150
120
90
60
30
0
0.2
1.0
1.8
1.8
1.8
1.8
1.0
0.2

while the activity at other hot spots may consist of sporadic or short-lived events.

6.1. *Persistent Hot Spots*

An important and somewhat surprising result from the Galileo observations is that many of Io's hot spots are active over periods of time ranging from months to years. It was known from groundbased observations that Loki is a persistently active hot spot, and that a few others such as Kanehekili and Hi'iaka are often active. The Galileo observations show that numerous other hot spots on Io also fall into this category. Although the lack of continuous temporal coverage introduces some uncertainty on whether these hot spots were active between consecutive detections, the Galileo observations show that the activity at these hot spots either was continuous (a single eruption) or consisted of frequent, intermittent events.

The hot spot detections by Galileo are listed in Table IV. For each hot spot, we list whether they were observed by either NIMS or SSI in any given orbit from G1 through C10, whether they were detected by either instrument, and whether they had been previously detected by Voyager or groundbased observations. We do not include the following active volcanic centers in this temporal analysis: hot spots not detected by Galileo, plume activity, and the marginal detection of Karei by SSI. The total number of hot spots considered in Table IV is therefore 40.

We note that 8 hot spots were active for periods of time ranging from 3 months to 1 year. These hot spots are Maui, 9606W, Volund, Fo, Sethlaus, Rata, Kurdalagon, 9611A, Babbar, and Amaterasu. A total of 22 hot spots were active over timescales longer than 1 year. Table V shows how often these 22 hot spots were observed and detected by NIMS and SSI. For each hot spot, we give the percentage of the number of Galileo orbits in which it was detected out of the number of Galileo orbits in which it was observed. Seven of the hot spots were detected in 100% of the orbits in which they were observed, showing that at least at these locations activity was most likely continuous. Of these 7 hot spots, 5 were detected by Voyager in 1979 (Pele, Marduk, Isum, Amirani, and the Prometheus plume). Hi'iaka, Kanehekili, and possibly Mulungu were detected from groundbased observations in the years between Voyager and Galileo. It is likely that activity at these hot spots (and possibly others not observed by Voyager IRIS) has persisted over several years, and perhaps some of them have been continuously active during the 17 years between Voyager and Galileo.

Is there a correlation between persistency of hot spot activity and plumes? We find that most of the known plumes that are associated with hot spots (excluding Ra and, for this analysis up to Galileo orbit C10, Masubi) were observed at the most persistent hot spots listed in Table V (9/12 or 75%). The only plume sites which do not coincide with the hot spots in Table V are the Voyager-observed plumes Maui and Volund, and the Galileo-observed Acala. Of these, Acala is the only hot spot that, up to orbit C10, was not observed to be active over timescales of at least 3 months, though results from orbits later than C10 indicate that it may also be a persistent hot spot. Red deposits are prominent at 50% of the persistent hot spots listed in Table V.

While persistent, the level of activity at the hot spots in Table V can vary significantly from orbit to orbit. The major changes detected by NIMS have been at Malik, Loki, and Pillan. Malik brightened between orbits G1 and G2, indicating an increase in temperature of at least 400 K (Lopes-Gautier *et al.* 1997b). Pillan brightened between orbits G7 and C9, accompanied by the appearance of a plume and a dramatic change in surface appearance observed by SSI (McEwen *et al.* 1998a). The Loki brightening between E6 and G7 was first reported by Spencer *et al.* [1997a] from groundbased observations. The brightening was clearly seen in a comparison between NIMS images from E6 and G7 (Fig. 9). In G7, NIMS observed Loki in darkness. NIMS data taken on Io's nightside were fitted to a Planck function to yield a best-fit blackbody temperature for the spectra from each pixel (see Lopes-Gautier *et al.* 1997a and Davies *et al.* 1997 for a description of the method). The temperature and area obtained were compared to the groundbased measurements (Fig. 10), indicating good agreement.

Less dramatic changes in activity were also observed by NIMS for other hot spots (Lopes-Gautier *et al.* 1999), with some hot spots brightening in terms of power output (e.g., Tupan between G1 and C9) and some fading (e.g., Altjirra from G1 to E11). It is possible that there are overall trends of brightening and fading for all of Io's persistent hot spots, and these may be revealed by further analysis of NIMS data from all orbits.

6.2. *Sporadic Events*

Hot spots that were detected less often than those in the persistent category *may* represent sites of sporadic, short-lived events. Alternatively, these hot spots may also be persistently active, but their activity may normally be at lower levels than can be detected by the majority of our observations. We have found nine

FIG. 9. The brightening of Loki during 1997 observed by NIMS during Galileo orbits E6 and G7. Loki is seen in daylight in E6, and near the terminator in G7. Both maps are at 2.9564 μm. In E6, the signal from Loki at this wavelength is not significantly above the background, though the signal at wavelengths longer than 3.5 μm is. After the brightening, Loki can be seen clearly above the background in the 2.9564-μm map from the G7 observation.

FIG. 11. Locations of hot spots plotted over the heat flow patterns predicted by the asthenosphere model (Ross *et al.* 1990). Persistent hot spots (filled orange circles) and active plumes (blue circles) are marked. Contours are in watts per meter squared. All persistent hot spots and active plumes are located within the 1-W m^{-2} regions and all are located at latitudes lower than 50°.

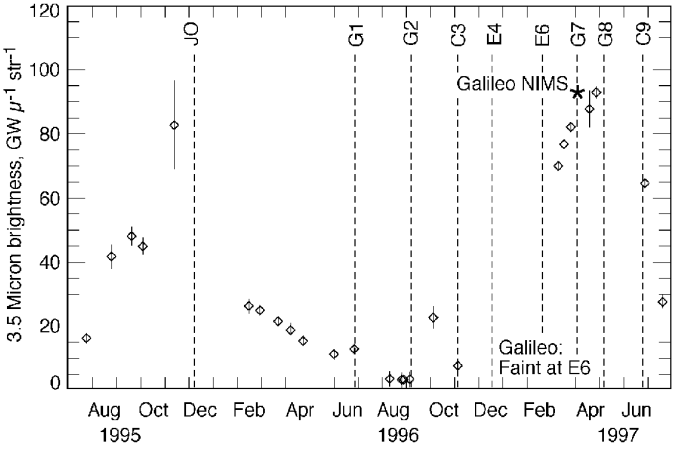

FIG. 10. Groundbased data by Spencer *et al.* (diamonds) show the variation in the 3.5-μm brightness of Loki from 1995 to 1997. NIMS observed Loki in darkness during orbit G7 and a single-temperature fit to the NIMS data (single asterisk) yields $T = 500$ K, area $= 1539$ km^2, consistent with the trend seen by the groundbased observations.

hot spots observed by Galileo that are in this category. The observed activity at these nine hot spots has lasted under 3 months. In the case of the Reiden hot spot that was only detected in the first orbit, G1, there is uncertainty to the duration of the active phase, because activity during the previous months was not known. Similarly, the duration of activity for hot spots only detected in C10 cannot be constrained until analysis of later orbits. These are the hot spot at (3N, 76W), Shamshu, and S. Sigurd.

The five hot spots where activity may indeed have been short-lived are the SSI-detected hot spot at (65N, 141W), Lei-Kung, Svarog, Daedalus, and Acala. Svarog, Daedalus, and Acala were detected by Voyager IRIS (and Acala was detected by Galileo after orbit C10); therefore we know that activity at those sites reoccurs over timescales of years, even if individual events are short lived. It is likely that the single NIMS detection of Lei-Kung reflects normally low levels of activity rather than short duration, because Lei-Kung was detected only during the highest resolution observation by NIMS. Observations by NIMS at equal or higher spatial resolution, planned during GEM, will better constrain the nature of this hot spot. SSI observations of hot spots are likely to show more variation than those by NIMS, because SSI detects only the hotter material (>700 K) from freshly emplaced lavas. This material is more temporally variable than the lower temperature materials, from cooling lavas, which can be detected by NIMS.

While at most five of the Galileo-observed hot spots could be characterized as sporadic events, several of the hot spots detected from the ground by Spencer *et al.* (1997a) during the Galileo monitoring phase (Table III) appear to be short-lived events. Galileo has not detected at least nine of these ground-observed hot spots (see Tables I and III). Three of these nine hot spots were observed by Spencer *et al.* (1997a) prior to the start of the main Galileo monitoring campaign on June 28, 1996, and six were observed during the Galileo campaign.

The 9503A event was an outburst and the hot spot persisted for several months. Outbursts are rare events (Spencer and Schneider 1996) and should be considered separately from either long-lived or sporadic activity. For the purposes of this analysis, we do not include 9503A as a sporadic event since it was observed more than once by Spencer *et al.* (1997a) over a period of several months. The 9507A and 9508A events were also observed more than once from the ground, and 9608A is possibly the same hot spot as 9508A. We consider the other five hot spots (9606E, 9606F, 9606G, 9606J, 9610A) to be possible sporadic events.

The hot spots 9606E, -F, -G, and -J were observed on June 2, 1996. NIMS and SSI observed Io on June 28 and 29, but the observations did not cover the longitudes of these hot spots. The first opportunity Galileo had to detect 9606E, -G, and -J was during a NIMS observation taken in orbit G2 on September 7, 1996. The first Galileo observation of the 9606F location was an eclipse image taken by SSI during orbit E4 on December 17, during which the longitudes of 9606E, -F, and -G were also observed. We can infer that the activity of 9606E, -G, and -J waned to levels below detection by NIMS and SSI in 3 months or less, while the activity at 9606F waned in 6 months or less. Because of the lack of Galileo observations prior to June 2, 1996, constraints on the total duration of activity at these hot spots cannot be obtained from Galileo data. Therefore, it is not clear that these are sporadic events according to our definition. However, lack of detection by Galileo during subsequent orbits, and by groundbased observations at any other time, implies that they may indeed have been short-lived.

Only one hot spot, 9610A, was detected from the ground between Galileo orbits. Limits on the duration of activity of this hot spot (at least at levels that can be detected by Galileo) can be obtained by using the dates of the Galileo observations. 9610A was observed from the ground on October 1, 1996. NIMS observations covering the same longitude taken on June 28, 1996, and on April 3, 1997, failed to show the hot spot, as did an SSI eclipse observation on December 17, 1996. The duration of the activity was therefore under 6 months. However, the high latitude of 9610A (70 ± 15) makes it somewhat less likely to be detected than low latitude events. It is possible that the hot spot persisted for longer, but the activity detected by Spencer *et al.* (1997a) may have corresponded to a phase when hypothesized high fire fountains were active, thus making the event possible to detect by observations which are essentially equatorial (Stansberry *et al.* 1997).

The fact that five possible sporadic events were detected by groundbased observations, compared with the same number observed by Galileo, stresses the importance of groundbased observations to monitor Io's activity. Telescopic sessions can observe Io for much longer periods than Galileo. Galileo observations are only a few minutes long, and only a few are typically taken in each Galileo orbit. It is clear that understanding the frequency and magnitude of sporadic events is essential for our understanding of Io volcanism, and that can only be accomplished by

frequent monitoring. Once the Galileo mission is over, groundbased observations will be the primary remaining resource for continuing to build our knowledge of the frequency of sporadic events.

7. SUMMARY, CONCLUSIONS, AND FUTURE WORK

The comparison between Galileo NIMS and SSI data from nine Galileo orbits with those taken from groundbased telescopes and by Voyager IRIS has revealed new insights into Io's global distribution of volcanism, the correlation of hot spots with surface features, and the temporal behavior of hot spots. Below we summarize our findings and discuss their implications.

7.1. Hot Spots, Surface Features, and Surface Colors

The comparison of hot spot locations with surface features has confirmed previous suggestions that hot spots are associated with low-albedo features. We find that the most common type of surface feature associated with active volcanic centers is a patera (usually a caldera), but others include fluctus and fissure-like features. The size and morphology of surface features still need to be correlated with hot spot type based on their temporal behavior (persistent or sporadic), and temperatures measured by NIMS and SSI.

Our analysis also supports previous conclusions that red deposits are associated with active volcanic centers and are possibly the fallout from plumes. Galileo monitoring can help constrain the lifetime of red deposits. At one site, Tohil Patera, no volcanic activity has been detected by Galileo, implying that red deposits last for at least 18 months.

We find that hot spots are generally anti-correlated with bright white deposits, which are known to be regions of high concentrations of SO_2 frost and low temperatures. While the anti-correlation between hot spots and cold SO_2 snowfields is expected, and supports the regional cold-trap model of Fanale *et al.* (1982), the geographical distribution of the snowfields has yet to be explained. Galileo SSI results (Thomas *et al.* 1998) do not support the existence of equatorial basins suggested from Voyager data (Gaskell *et al.* 1988, McEwen 1995), which were interpreted from Voyager to be SO_2-rich. Future work involving global thermal maps from NIMS data and a global topographic map from SSI data will seek to clarify if the distribution of cold, bright white regions and local concentrations of hot spots reflect the distribution of internal heating or local differences in crustal thickness as proposed by Ross *et al.* [1990].

7.2. Temporal Behavior of Hot Spots

We find that Io's hot spots can be persistently active over timescales of months to years. Our results show that 8 hot spots were active over timescales of 3 months to at least one year, while the activity at 22 hot spots lasted for longer than one year, possibly much longer. Sporadic events also occur, and may represent short-lived activity or activity that is mostly at levels below the detection limits of the instruments. The contribution of these two types of activity to Io's global volcanism has yet to be assessed. Galileo data show that 5 hot spots may have been sporadic, while groundbased observations reveal 5 other hot spots that may also fall in this category.

It is possible that all hot spots on Io are long-lived, but activity at the sporadic sites is normally at levels sufficiently low so that they cannot be detected by Galileo's instruments. Since activity at a hot spot may always be present at levels below detection, it is not practical to attempt to differentiate between the two categories of hot spots in terms of *actual duration of all activity*. However, the two types of hot spots are clearly different in terms of *duration of the vigorous active phase that can be detected by Galileo*. An important question is whether the persistent (or vigorous) and sporadic (short-lived or normally low-level) types of activity imply different types of volcanoes on Io, perhaps in terms of rate of magma supply, internal plumbing, or magma composition. If so, morphological differences may be present, but these are hard to characterize at present because of the small number of sporadic type hot spots known.

An important question raised by the temporal behavior of hot spots is since levels of activity at all hot spots can fall to levels that cannot be detected by the currently available instruments, how many more active hot spots are there on Io? Would their number and distribution significantly change our current results?

Although the hot spots in the persistent category are clearly more likely to have been detected in the current data set than hot spots in the sporadic category, it is doubtful that we have detected all of the persistent hot spots. Apart from constraints imposed by the relatively short duration of Galileo's monitoring phase and by the wavelength range of the instruments, there are also observational constraints. The bulk of the Galileo monitoring observations were carried out by NIMS, and NIMS observations had particularly low spatial resolution from longitudes 350W–0–40W. Therefore, it is not surprising that no persistent hot spots were observed within those longitudes. It is thus possible that a greater number of hot spots in this category are present close to the subjovian point.

Sporadic events are clearly less likely to be detected, either because of their short duration or because the activity is normally at low levels and only occasionally flares up. An important conclusion drawn from the temporal analysis is that these sporadic events do occur on Io, and can go largely undetected because the frequency of monitoring has been mostly on the scale of several months. The distribution of the sporadic hot spots is therefore largely unknown, as is their relative contribution to Io's heat flow. The conclusions drawn from our current set of observations are based largely on the distribution of persistent-type hot spots.

7.3. Global Distribution of Active Volcanic Centers

The combination of NIMS, SSI, groundbased, and Voyager IRIS data shows that there are at least 61 hot spots on Io, plus 2 plume sites where no hot spot has yet been detected, and an

additional 25 probable active volcanic centers. It is important to note that NIMS and SSI cannot detect relatively low-temperature hot spots (below about 200 K) that may make an important contribution to the dissipation of Io's internal heat. It is not, however, unreasonable to assume that the heat flow distribution at Io's surface may be proportional to the heat flow detected by NIMS and SSI. Therefore, the hot spots detected by these instruments, plus those detected by Voyager and groundbased observations, may well reflect the first-order, overall distribution of heat flow on Io's surface.

Our analysis shows that the distribution of active volcanic centers (hot spots plus two plumes sites) appears to be fairly uniform with respect to latitude and longitude. No correlation with global topography (derived from Voyager data) has been found, but this result will need to be reexamined when improved models of topography become available. The distribution of active volcanic centers is not well correlated with predictions of surface heat flow patterns derived from the asthenosphere and deep mantle tidal dissipation models (Segatz *et al.* 1988, Ross *et al.* 1990), though the typical separations between active volcanic centers and the apparent deficit of centers at high latitudes are consistent with the asthenosphere model.

7.4. Implication of Temporal Behavior of Hot Spots to Global Distribution and to Io's Heat Flow

We can further examine how the distribution of active volcanic centers may reflect internal heating mechanisms by taking into account differences in temporal behavior (persistent versus sporadic) of hot spots, and the presence or absence of plumes. Figure 11 shows the distribution of hot spots overlaid on the heat flow pattern predicted by the asthenosphere tidal heating model, with the locations of plumes and persistent hot spots highlighted. It is clear that both plumes and persistent hot spots are concentrated toward lower latitudes. All persistent hot spots are located at latitudes lower than 50°, in regions where the predicted heat flow on the surface is greater than 1 W m^{-2}.

This result provides added support for the asthenosphere model, because persistent hot spots are likely to represent the current major pathways of magma from Io's interior to the surface. The predominance of plumes near the equator (McEwen *et al.* 1998a) could reflect a correlation between plumes and persistent hot spots.

Hot spots also differ from one another in terms of power output, and the effect of this factor on the global distribution of hot spots is being examined by Smythe *et al.* (1999) using NIMS data. Preliminary results show that hot spots having the largest power output are also concentrated toward the equator.

Our results, therefore, favor the asthenosphere tidal dissipation model over the deep-mantle model. However, this conclusion is based on the premise that the hot spots detected by Galileo, groundbased instruments, and Voyager IRIS are representative of the global distribution of all hot spots on Io, including low-temperature thermal anomalies.

7.5. Activity at Persistent Hot Spots

Galileo's long-term monitoring of hot spots can reveal possible differences among persistent hot spots, and changes in their levels of activity, that are important for characterizing Io's predominant eruption mechanisms.

SSI and NIMS are able to detect different phases (or possibly different types) of hot spot activity. Both instruments are able to detect bright, high-temperature hot spots such as Pele and Pillan. These are sites of very vigorous activity where a hot component is being frequently exposed at the surface. High temperatures measured at several of these hot spots, such as Pillan (McEwen *et al.* 1998b), imply that the magmas are ultramafic in composition, possibly analogous to terrestrial komatiites. Our knowledge of the eruption processes of komatiites is limited because these eruptions rarely occurred on Earth since the Archean. One important consideration for modeling the emplacement of lava flows on Io is that terrestrial komatiites are thought to have been emplaced as turbulent flows (Huppert *et al.* 1987, Huppert and Sparks 1985). The majority of current lava flow emplacement models are based on the behavior of laminar flow.

The longer wavelength range of NIMS compared to that of SSI allows it to detect lower temperature hot spots. The "cooler" hot spots detected only by NIMS (e.g., Hi'iaka and Sigurd) may represent a type or stage of activity in which a high-temperature component (above 700 K) is either small in area or absent. This could be the case for a lava lake or flow that has a relatively cool crust over large parts of its area. Alternatively, it is possible that the magma being erupted at these hot spots is lower in temperature, perhaps implying different composition. We expect to be able to clarify these possibilities by doing more detailed analysis of the shorter wavelength data in the NIMS spectra. For example, fitting two or three temperatures to NIMS spectra (e.g., McEwen *et al.* 1998, Davies *et al.* 1999) can reveal high-temperature components of individual hot spots, provided the area is sufficiently large to be detected at NIMS spatial resolutions. Further measurements by SSI will also search for hot components at different times over the Galileo observing period. If high temperatures consistent with ultramafic volcanism are widespread on Io, then the crust could be mafic. If high-temperature volcanism is relatively rare, then Io's crust could be more evolved.

Significant variations in the level of activity of Io's persistent hot spots are known to occur. For example, dramatic variations in hot spot activity at Loki have been long known from groundbased data. Future detailed analysis of Galileo's numerous observations of persistent hot spots may reveal brightening and waning patterns that may be indicative of temporal changes in the rate of magma supply.

Understanding the behavior of persistent-type hot spots, including their overall eruption rates, can give us insights into the mechanisms involved in the transfer of magma from Io's interior to the surface. It is known that long-lived eruptions on Earth can last for decades (e.g., Simkin and Siebert 1994). Recent examples for which the infrared signature is well documented

include the 1983 to present eruption of Pu'u O'o in Hawaii, dominated by numerous lava flows (e.g., Flynn and Mouginis-Mark 1992) and the 1984 to 1995 eruption from a dome within the active crater of Lascar, Chile (Wooster and Rothery 1997). Much longer timescales of volcanic activity are known on Earth, up to the 2500 years of nearly continuous activity at Stromboli. "Steady-state" volcanism on Earth occurs when the magma eruption rate is balanced by the magma supply rate. Therefore, measurements of the magma eruption rate can be used to estimate the minimum magma supply rate (e.g., Sigurdsson and MacDonald 1999, Harris *et al.* 1999, Oppenheimer and Francis 1997). Future work will take advantage of the many observations obtained by NIMS of persistent hot spots to measure temporal variations in temperature and area, from which a range of eruption rates can be calculated using plausible thicknesses. These values can then be used to estimate the minimum magma supply rate to the surface at the present state of Io's volcanism.

7.6. Future Observations

Further observations by Galileo during the Galileo Europa Mission (1998–2000) and from groundbased telescopes will continue to build up our knowledge of the types and temporal variability of hot spots on Io. Since Galileo has made few observations of Io during most of GEM, groundbased observations have been essential for continuing the study of the temporal variability of Io's hot spots. Galileo will obtain very high spatial resolution observations of Io at the end of GEM (down to 200 m/pixel for NIMS and about 5 m/pixel for SSI). Areas targeted include inferred locations of volcanic vents, active plumes, and samples of red, green, and dark materials. Although the temporal coverage will be small, these Galileo observations will, for the first time, show details of the morphology, thermal structure and composition of Io's active volcanic centers.

ACKNOWLEDGMENTS

We thank Robert Howell and David Rothery for helpful reviews; and Elias Barbinis, Marcia Segura, Jim Shirley, Paul Herrera, and the Galileo team at JPL for support with sequencing and data downlink activities. Our work has greatly benefitted from discussions with other members of the ad-hoc Io Working Group. The Galileo Project is funded by the Nasa Solar System Exploration Division. The work described here was performed at the Jet Propulsion Laboratory, California Institute of Technology, under contract with NASA.

REFERENCES

Belton, M. J. S., and 22 colleagues 1992. The Galileo solid-state imaging experiment. *Space Sci. Rev.* **60**, 413–456.

Blaney, D. L., T. V. Johnson, D. L. Matson, and G. J. Veeder 1995. Volcanic eruptions on Io: Heat flow, resurfacing, and lava composition. *Icarus* **113**, 220–225.

Carlson, R. W., W. D. Smythe, R. Lopes-Gautier, A. G. Davies, L. W. Kamp, J. A. Mosher, L. A. Soderblom, F. E. Leader, R. Mehlman, R. N. Clark, and F. P. Fanale 1997. The distribution of sulfur dioxide and other infrared absorbers on the surface of Io in 1997. *Geophys. Res. Lett.* **24**, 2479–2482.

Carlson, R. W., P. R. Weissman, W. D. Smythe, J. C. Mahoney, and the NIMS Science and Engineering Teams 1992. Near infrared spectrometer experiment on Galileo. *Space Sci. Rev.* **60**, 457–502.

Carr, M. H., A. S. McEwen, K. A. Howard, F. C. Chuang, P. Thomas, P. Schuster, J. Oberst, G. Neukum, G. Schubert, and the Galileo Imaging Team 1998. Mountains and calderas on Io: Possible implications for lithosphere structure and magma generation. *Icarus* **135**, 146–165.

Davies, A. G., R. Lopes-Gautier, W. D. Smythe, and R. W. Carlson 1999. Multiple-temperature fits to Galileo NIMS data of volcanism on Io. *Icarus*, submitted.

Davies, A. G., A. S. McEwen, R. Lopes-Gautier, L. Keszthelyi, R. W. Carlson, and W. D. Smythe 1997. Temperature and area constraints of the S. Volund Volcano on Io from the NIMS and SSI instruments during the Galileo G1 orbit. *Geophys. Res. Lett.* **24**, 2447–2450.

Fanale, F. P., W. P. Banerdt, L. S. Elson, T. V. Johnson, and R. W. Zurek 1982. Io's surface: Its phase composition and influence on Io's atmosphere and Jupiter's magnetosphere. In *Satellites of Jupiter* (D. Morrison, Ed.), pp. 756–781. Univ. of Arizona Press, Tucson.

Flynn, L. P., and P. J. Mouginis-Mark 1992. Cooling rate of an active Hawaiian flow from nighttime spectroradiometer measurements. *J. Geophys. Res.* **19**, 1783–1786.

Gaskell, R. W., S. P. Synnott, A. S. McEwen, and G. G. Schaber 1988. Large-scale topography of Io: Implications for internal structure and heat transfer. *Geophys. Res. Lett.* **15**, 581–584.

Geissler, P. E., A. S. McEwen, L. Keszthelyi, R. Lopes-Gautier, J. Granahan, and D. P. Simonelli 1999. Global color variations on Io. *Icarus* **140**, 265–282.

Goguen, J. D., W. M. Sinton, D. L. Matson, R. R. Howell, H. M. Dyck, T. V. Johnson, R. H. Brown, G. J. Veeder, A. L. Lane, R. M. Nelson, and R. A. McLaren 1988. Io's hot spots: Infrared photometry of satellite occultations. *Icarus* **76**, 465–484.

Harris, A. J. L., L. P. Flynn, D. A. Rothery, C. Oppenheimer, and S. B. Sherman 1999. Mass flux measurements at active lava lakes: Implications for magma recycling. *J. Geophys. Res.*, in press.

Huppert, H. E., R. S. J. Sparks, J. S. Turner, and N. T. Arndt. Emplacement and cooling of komatiite lavas. *Nature* **309**, 19–22, 1987.

Huppert, H. E., and R. S. J. Sparks. Komatiites: Eruption and flow. *J. Petrol.* **26**, 694–725, 1985.

Johnson, T. V., G. J. Veeder, D. L. Matson, R. H. Brown, R. M. Nelson, and D. Morrison 1988. Io: Evidence for silicate volcanism in 1986. *Science* **242**, 1280–1283.

Kerton, C. R., F. P. Fanale, and J. R. Salvail 1996. The state of SO_2 on Io's surface. *J. Geophys. Res.* **101**, 7555–7563.

Klaasen, K. P., and 15 colleagues 1997. Inflight performance characteristics, calibration, and utilization of the Galileo SSI camera. *Opt. Eng.* **38**, 3001–3027.

Lopes-Gautier, R., A. G. Davies, R. Carlson, W. Smythe, L. Kamp, L. Soderblom, F. E. Leader, R. Mehlman, and the Galileo NIMS Team 1997a. Hot spots on Io: Initial results from the Galileo near-infrared mapping spectrometer. *Geophys. Res. Lett.* **24**, 2439–2442.

Lopes-Gautier, R., A. G. Davies, R. Carlson, W. Smythe, and L. Soderblom 1997b. Monitoring of Io's volcanic activity using Galileo's near infrared mapping spectrometer (NIMS). *Proc. Lunar Planet. Sci. Conf. 28th*, 831.

Lopes-Gautier, R., W. D. Smythe, A. S. McEwen, P. E. Geissler, A. G. Davies, L. Kamp, L. A. Soderblom, R. W. Carlson, L. Keszthelyi, J. R. Spencer, and the Galileo NIMS Team 1999. The temporal activity of Io's hot spots. *Proc. Lunar Planet. Sci. 30th*. [Available on CD-Rom]

McEwen, A. S. 1995. SO_2-rich equatorial basins and epeirogeny of Io. *Icarus* **113**, 415–422.

McEwen, A. S., N. R. Isbell, K. E. Edwards, and J. C. Pearl 1992b. New Voyager 1 hot spot identifications and the heat flow of Io. *Bull. Am. Astron. Soc.* **24**, 935.

McEwen, A. S., N. R. Isbell, and J. C. Pearl 1992a. Io thermophysics: New models with Voyager 1 thermal IR spectra. *Proc. Lunar Planet. Sci. Conf. 23rd*, 881.

McEwen, A. S., J. I. Lunine, and M. H. Carr 1989. Dynamic Geophysics of Io. In *Time-Variable Phenomena in the Jovian System* (M. J. S. Belton, R. A. West, and J. Rahe, Eds.), pp. 11–46. NASA S-P 494, Washington, DC.

McEwen, A. S., D. Simonelli, D. Senske, K. Klaasen, L. Keszthelyi, T. Johnson, P. Geissler, M. Carr, and M. Belton 1997. High temperature hot spots on Io as seen by Galileo's Solid State Imaging (SSI) Experiment. *Geophys. Res. Lett.* **24**, 2443–2446.

McEwen, A. S., and 13 colleagues 1998a. Active volcanism on Io as seen by Galileo SSI. *Icarus* **135**, 181–219.

McEwen, A. S., and 14 colleagues 1998b. High temperature silicate volcanism on Jupiter's moon Io. *Science* **281**, 87–90.

Moses, J. I., and D. B. Nash 1991. Phase transformations and spectral reflectance of solid sulfur: Can metastable sulfur allotropes exist on Io? *Icarus* **89**, 277–304.

Oppenheimer, C., and P. Francis 1997. Remote sensing of heat, lava, and fumarole emissions from Erta'Ale volcano, Ethiopia. *Int. J. Remote Sensing* **98**, 4269–4286.

Pearl, J., and W. M. Sinton 1982. Hot spots of Io. In *Satellites of Jupiter* (D. Morrison, Ed.), pp. 724–755. Univ. Ariz. Press, Tucson.

Ross, M. N., G. Schubert, T. Spohn, and R. W. Gaskell 1990. Internal structure of Io and the global distribution of its topography. *Icarus* **85**, 309–325.

Schubert, G., P. J. Tackley, J. P. Matas, G. A. Glatzmaier, and J. T. Ratcliff 1998. Three-dimensional numerical simulations of mantle convection in Io. *Eos* (Fall Supplement) **79**, F529.

Segatz, M., T. Spohn, M. N. Ross, and G. Schubert 1988. Tidal dissipation, surface heat flow, and figure of viscoelastic models of Io. *Icarus* **75**, 187–206.

Sigurdsson, H., and R. MacDonald 1999. Geologic history of the Soufriere St. Vincent volcano. *Bull. Volcanol.*, in press.

Simkin, T., and L. Siebert 1994. *Volcanoes of the World*, Second ed. Smithsonian Institution, Geoscience Press, Tucson.

Simonelli, D. P., Veverka, J., and A. S. McEwen 1997. Io: Galileo evidence for major variations in regolith properties. *Geophys. Res. Lett.* **24**, 2475–2478.

Sinton, W. M. 1980. Io's 5-micron variability. *Astrophys. J.* **235**, L49–51.

Smith, B. A., and the Voyager Imaging Team 1979. The Jupiter system through the eyes of Voyager 1. *Science* **204**, 951–972.

Smythe, W. D., R. Lopes-Gautier, A. Davies, R. Carlson, L. Kamp, L. Soderblom, and the Galileo NIMS Team 1997. A temperature distribution map of Io from Galileo's near-infrared mapping spectrometer (NIMS). In *Io during the Galileo Era*, p. 14. Lowell Observatory, Flagstaff, AZ.

Smythe, W. D., R. Lopes-Gautier, L. Kamp, A. G. Davies, R. W. Carlson, L. A. Soderblom, and the Galileo NIMS Team 1999. Io thermal output distribution from Galileo's near-infrared mapping spectrometer (NIMS). *Proc. Lunar Planet. Sci. Conf. 30th*. [Available on CD-Rom]

Smythe, W. D., and 14 colleagues 1995. Galilean satellite observation plans for the near-infrared mapping spectrometer on the Galileo spacecraft. *J. Geophys. Res.* **100**, 18,957–18,972.

Spencer, J. R., and N. M. Schneider 1996. Io on the eve of the Galileo mission. *Annu. Rev. Earth Planet. Sci.* **24**, 125–190.

Spencer, J. R., A. S. McEwen, M. A. McGarth, P. Sartoretti, D. B. Nash, K. S. Noll, and D. Gilmore 1997b. Volcanic resurfacing of Io: Post-repair HST imaging. *Icarus* **127**, 221–237.

Spencer, J. R., P. Sartoretti., G. E. Ballester, A. S. McEwen, J. T. Clarke, and M. McGarth 1997c. The Pele plume (Io): Observations with the Hubble Space Telescope. *Geophys. Res. Lett.* **24**, 2471–2474.

Spencer, J. R., J. A. Stansberry, C. Dumas, D. Vakil, R. Pregler, and M. Hicks 1997a. A history of high-temperature Io volcanism, February 1995 to May 1997. *Geophys. Res. Lett.* **24**, 2451–2454.

Stansberry, J. A., J. R. Spencer, R. R. Howell, C. Dumas, and D. Vakil 1997. Violent silicate volcanism on Io in 1996. *Geophys. Res. Lett.* **24**, 2455–2458.

Strom, R. G., N. M. Schneider, R. J. Terrile, A. F. Cook, and C. Hansen 1981. Volcanic eruptions on Io. *J. Geophys. Res.* **86**, 8593–8620.

Thomas, P. C., M. E. Davies, T. R. Colvin, J. Oberst, P. Schuster, G. Neukum, M. H. Carr, A. McEwen, G. Schubert, M. J. S. Belton, and the Galileo Imaging Team 1998. The shape of Io from Galileo limb measurements. *Icarus* **135**, 175–180.

Veeder, G. J., D. L. Matson, T. V. Johnson, D. L. Blaney, and J. D. Goguen 1994. Io's heat flow from infrared radiometry: 1983–1993. *J. Geophys. Res.* **99**, 17,095–17,162.

Wooster, M. J., and D. A. Rothery 1997. Thermal modelling of Lascar volcano, Chile, using infrared data from the along-track scanning radiometer: A 1992–1995 time series. *Bull. Volcanol.* **58**, 566–579.